Monthly Notices
of the
ROYAL ASTRONOMICAL SOCIETY

MNRAS **457,** 1107–1123 (2016) doi:10.1093/mnras/stw028

Progenitor constraints for core-collapse supernovae from *Chandra* X-ray observations

T. Heikkilä,[1★] S. Tsygankov,[1] S. Mattila,[1,2,3] J. J. Eldridge,[4] M. Fraser[3] and J. Poutanen[1]

[1] *Tuorla Observatory, Department of Physics and Astronomy, University of Turku, Väisäläntie 20, FI-21500 Piikkiö, Finland*
[2] *Finnish Centre for Astronomy with ESO (FINCA), University of Turku, Väisäläntie 20, FI-21500 Piikkiö, Finland*
[3] *Institute of Astronomy, University of Cambridge, Madingley Road, Cambridge CB3 0HA, UK*
[4] *Department of Physics, University of Auckland, Private Bag 92019, Auckland, New Zealand*

Accepted 2016 January 4. Received 2016 January 4; in original form 2015 November 2

Downloaded from http://mnras.oxfordjournals.org/ at University of Turku on February 1, 2016

ABSTRACT

The progenitors of hydrogen-poor core-collapse supernovae (SNe) of Types Ib, Ic and IIb are believed to have shed their outer hydrogen envelopes either by extremely strong stellar winds, characteristic of classical Wolf–Rayet stars, or by binary interaction with a close companion star. The exact nature of the progenitors and the relative importance of these processes are still open questions. One relatively unexplored method to constrain the progenitors is to search for high-mass X-ray binaries (HMXBs) at SN locations in pre-explosion X-ray observations. In an HMXB, one star has already exploded as a core-collapse SN, producing a neutron star or a stellar mass black hole. It is likely that the second star in the system will also explode as an SN, which should cause a detectable long-term change in the system's X-ray luminosity. In particular, a pre-explosion detection of an HMXB coincident with an SN could be informative about the progenitor's nature. In this paper, we analyse pre-explosion ACIS observations of 18 nearby Type Ib, Ic and IIb SNe from the *Chandra* X-ray observatory public archive. Two sources that could potentially be associated with the SN are identified in the sample. Additionally we make similar post-explosion measurements for 46 SNe. Although our modelling indicates that progenitor systems with compact binary companions are probably quite rare, studies of this type can in the future provide more stringent constraints as the number of discovered nearby SNe and suitable pre-explosion X-ray data are both increasing.

Key words: binaries: close – stars: evolution – supernovae: general – supernovae: individual: SN 2004gt – stars: Wolf–Rayet – X-rays: binaries.

1 INTRODUCTION

Supernovae (SNe) are broadly divided into two classes based on the presence (Type II) or absence (Type I) of strong hydrogen features in their spectrum (e.g. Filippenko 1997). SNe other than Type Ia are believed to be the result of core-collapse explosions of massive stars at the end of their lifespan. Among hydrogen-poor core-collapse supernovae (CCSNe), the lack of H-features in their spectra is attributed to these stars having lost their hydrogen envelope prior to the explosion, and hence are collectively referred to as stripped-envelope CCSNe. These are SN Types Ib, Ic and also IIb (which, while they show H-features initially, rapidly lose them and begin to display He-features instead). There are believed to be two primary channels to produce stripped-envelope CCSNe, both of which are likely to be responsible for producing some fraction of these SNe.

Previously, the preferred model was that the progenitors were single Wolf–Rayet (WR) stars with initial masses above $\sim$25 $M_{\odot}$, characterized by high mass-loss rates, resulting in their envelopes being lost through radiatively driven winds (see e.g. Crowther 2007, for review). However, recently the alternative mechanism for producing a stripped-envelope SN progenitor, binary interaction, has become the more favoured explanation. In an interacting binary scenario, a progenitor that is not sufficiently massive to enter a WR-stage by itself could none the less lose its hydrogen envelope either by Roche lobe overflow to a close companion star or via common-envelope evolution (Podsiadlowski, Joss & Hsu 1992). In fact, based on the studies by e.g. Podsiadlowski et al. (1992), Vanbeveren et al. (1998), Smith et al. (2011) and Eldridge et al. (2013), the high relative rate[1]

[1] According to a study by Eldridge et al. (2013, based on a sample of 100 nearby SNe) 26 per cent of CCSNe are of Type Ibc and 12 per cent Type IIb in a volume-limited sample (the remaining 62 per cent are non-stripped-envelope CCSNe such as Type IIP).

★E-mail: ttheik@utu.fi

© 2016 The Authors
Published by Oxford University Press on behalf of the Royal Astronomical Society

of Type Ibc SNe could not be reconciled with a single-star scenario where stellar wind dominates the removal of the envelope, and that classical WR-stars could not account for more than half of the observed Type Ibc SNe. Instead, the interacting binary scenario was found to be the more likely mechanism for most Type Ib and IIb (and large fraction of Ic) SN progenitors. Furthermore, Lyman et al. (2014) analysed the ejecta-masses of 36 stripped-envelope CCSNe and found that all but three of them were inconsistent with massive progenitor stars, which further supports the likelihood of less massive binary progenitors and suggests this might even be the dominant progenitor mechanism for stripped-envelope CCSNe. It should also be noted that there is a distinct lack of pre-explosion high-mass SN progenitor star detections (with initial mass above $\sim$18 $M_{\odot}$; Smartt 2015). It has been suggested that this lack is caused by failed SNe where the core of the star collapses directly into a black hole without detectable SN (see e.g. Gerke, Kochanek & Stanek 2015; Reynolds, Fraser & Gilmore 2015). This would reduce the population of massive stars available as potential single WR-star SN progenitors. For a more detailed discussion on the various progenitor models, see e.g. the recent review by Yoon (2015).

While a number of SN Type II-P progenitor stars have been directly identified in optical pre-explosion observations (see Smartt 2009, for review), only three Type IIb progenitors have been identified: SN 2008ax (Crockett et al. 2008), SN 1993J (Aldering, Humphreys & Richmond 1994; Maund & Smartt 2009) and SN 2011dh (Maund et al. 2011; Van Dyk et al. 2011), and only one Type Ibc progenitor with the recent discovery of the progenitor candidate for the Type Ib SN iPTF13bvn by Cao et al. (2013). The progenitor of SN 2008ax is the only one of these where a single WR-star progenitor cannot be ruled out, although a binary system seems to be the more likely possibility (see discussion in Smartt 2009 and also Crockett et al. 2008 and Roming et al. 2009). The progenitor of SN 1993J has been characterized by direct pre-explosion imaging to have been a red supergiant in a binary system. The progenitor of SN 2011dh was likewise identified by direct observation as a yellow supergiant in a probable binary system (Maund & Smartt 2009; Maund et al. 2011; Folatelli et al. 2014). The Type Ib SN iPTF13bvn is also now believed to have had a binary progenitor, the single massive WR-star scenario having been ruled out by Eldridge et al. (2015), Bersten et al. (2014), Fremling et al. (2014) and Kuncarayakti et al. (2015). Studies of the observed properties of Type IIb SNe have also been used to constrain their progenitors. For example, Bufano et al. (2014) found the progenitor of the Type IIb SN 2011hs to be consistent with a supergiant star with an initial mass less than 20 $M_{\odot}$ as also found for SNe 1993J and 2011dh. Based on radio observations, Ryder et al. (2004) suggest the progenitor to the Type IIb SN 2001ig was a WR-star in a binary, and the likely companion star has been identified as a late-B through late-F type supergiant (Ryder, Murrowood & Stathakis 2006).

In X-ray frequencies, there has been some effort to identify or constrain the properties of stripped-envelope CCSN progenitors. For example, Modjaz et al. (2009) and more recently Svirski & Nakar (2014) studied the shock breakout of SN 2008D and found its progenitor to be consistent with a WR-star. In a case study for the Type Ib SN 2010O in Arp299, Nelemans et al. (2010) used archival pre-explosion *Chandra* data and claimed the detection of a variable X-ray source coincident with the SN by comparing two observations taken at different times in order to estimate the flux. They suggested this might be indicative of the SN having a high-mass X-ray binary (HMXB) as a progenitor. An HMXB is a binary system consisting of a massive star which is losing mass to a compact companion, with accompanying X-ray emission. Similarly, Voss et al. (2011) noted the coincidence of the Type Ib SN 2009jf with the position of the ultraluminous X-ray source (ULX) CXOU J230453.0+121959, suggesting the possibility that the ULX may be a HMXB progenitor for the SN although they also note that a chance superposition is not unlikely. In this paper, we aim to extend the search for possible HMXB progenitors for stripped-envelope CCSNe in X-rays. Nielsen et al. recently carried out two studies in which they measured the X-ray luminosity at the sites of 13 Type Ia SNe, establishing upper limits for their progenitors (see Nielsen, Voss & Nelemans 2012, 2013). Here we make use of the overall methods of these two studies, but using a sample of SNe of Types Ib, Ic and IIb instead of Ia.

The Type IIb SNe with pre-explosion progenitor detections (SN 1993J, SN 2008ax and SN 2011dh, as well as the SNe with indirect progenitor constraints, SN 2001ig and SN 2011hs) were also included in this study for comparison. For iPTF13bvn no suitable *Chandra* observations were found and it was therefore excluded. We mainly focus on pre-explosion observations. Based on observed SN X-ray light curves the X-ray luminosity of a CCSN can be expected to remain relatively high for many years after the explosion due to the expansion of the SN ejecta into the circumstellar material (see e.g. Dwarkadas & Gruszko 2012), which is the principal source of X-rays during this phase. However, we have also included a large sample of post-explosion results in order to present a more complete picture. Although the main intent is to search for the progenitor of the second SN in a system that already contains a compact object (neutron star or a stellar mass black hole), it is quite possible that some of the SNe studied here could also have been the initial SN in the close binary system that resulted in a formation of an HMXB. Some of the SNe in our sample already had previously published luminosities or upper limits derived from the same post-explosion data. In particular, Perna et al. (2008) reported X-ray luminosities or their upper limits from post-explosion observations of 100 CCSNe of all types from *Chandra*, *XMM–Newton* and *Swift* to study a link between X-ray luminosity and the rotation speeds of pulsars at birth. However, because these previously published values are typically measured using a different selection of observations, energy range, assumed spectral model or aperture, they are not directly comparable to the results presented in this study.

In this paper, we use the following structure: In Section 2, we cover our sample selection and the observations used in this study. In Section 3, we explain the processes we used for our data analysis, describe the spectral models used, and explain how the results were obtained. In Section 4, we examine the results in detail, consider the theoretical fraction of X-ray bright progenitor systems and present a prediction for the upper limits that can be obtained for future nearby SNe. Finally, in Section 5 we discuss some of the implications these results have for future studies of this type, followed by brief conclusions in Section 6.

2 OBSERVATIONS

Chandra X-ray observatory, launched in 1999, carries two instruments [High Resolution Camera (HRC) and Advanced CCD Imaging Spectrometer (ACIS)], and has a spatial resolution of $\sim$0.5 arcsec, although the point spread function (PSF) depends highly on photon energy and distance from the optical axis. Only ACIS observations were included in this study. ACIS is sensitive in the 0.3–8 keV energy range. The precision of the absolute astrometry of

Downloaded from http://mnras.oxfordjournals.org/ at University of Turku on February 1, 2016

Chandra data is sufficient for our study, with coordinate offsets being ∼1 arcsec or less in most instances.[2]

We selected from the Asiago SN catalogue (Barbon et al. 1999) all CCSNe (as of 2015 May 27) of Types Ib, Ic and IIb discovered after 1980 to ensure reasonably accurate astrometry. We then cross-correlated the known SN positions with *Chandra* archival data to find observations with ACIS data from either before or after the SN explosion. We removed from the sample all SNe with distance more than 100 Mpc. Some SNe were also removed from the sample due to data quality (SN near or outside detector edge, SN more than 10 arcmin from optical axis). To confirm that we were not missing a number of SNe without an International Astronomical Union (IAU) SN designation we also checked the 'Latest Supernovae' webpage (Gal-Yam et al. 2013) [3] for objects between 2013 and 2015 fulfilling the above criteria. A total of 31 such SNe were found, none of which had suitable ACIS data. This way, we found that suitable archival ACIS data were available for approximately 18 per cent of SNe within our search criteria. In total, 57 SNe were selected for the sample, of which 11 had only pre-explosion data available, seven had both pre- and post-explosion data and the remaining 39 post-explosion data only. The full list of all SNe included in the study and the *Chandra* observations used for each target are presented in Table 1, along with SN optical maximum or discovery dates (from Asiago) and the combined exposure times for both pre- and post-explosion categories.

All SN coordinates from Asiago were compared to both the Unified Supernova Catalogue (USC) (Lennarz, Altmann & Wiebusch 2012) and the Sternberg Supernova Catalogue (SSC) (Tsvetkov, Pavlyuk & Bartunov 2004). Whenever there were significant differences in the SN positions between Asiago and the other two catalogues,[4] we attempted to find a different source (see Tables 3 and 4) for the position. In all cases, adjustments were made if more accurate astrometry was available, even if the catalogues were in agreement.

In cases where multiple *Chandra* observations were found for a particular SN, all of the available data were first aligned. The data were then divided into pre- and post-explosion data sets for each SN. If any observation was made within several months of the SN date listed in Asiago catalogue[5] and there was a possibility of incorrectly assigning an observation to pre- or post-explosion data set, we ensured the categorization was correct by searching for (or narrowing down) the actual SN explosion date wherever possible. All pre- or post-explosion observations were then combined together to obtain the best possible signal-to-noise (S/N) ratio. Some observations were excluded however, either because their relatively short exposure times of < 5 ks would not have made any significant contribution to the total exposure time of the combined observation, or any data that were otherwise unsuitable, such as observations taken in *Chandra's* continuous-clocking mode. The observations, whether combined or single, were then used to obtain the flux and luminosity at the position of the SN before and/or after the explosion, or an upper limit where no source was detected (as was the case for most SNe).

[2] For details, see http://cxc.harvard.edu/cal/ASPECT/celmon/.

[3] http://www.rochesterastronomy.org/snimages/

[4] Differences less than ∼1 arcsec between the catalogues were not considered significant. Overall, the more recent USC was considered more accurate, and in case of discrepancies, if more accurate astrometry was not available we adopted the USC position instead.

[5] Asiago catalogue max. epoch: the date of optical maximum or discovery.

3 DATA ANALYSIS

We calculated luminosity for three simple spectral models approximating common properties of HMXBs (Mitsuda et al. 1984; Maccarone et al. 2014): a blackbody at the temperature of 1 keV (a black hole in soft state; accretion disc), a power law with photon index $\Gamma = 0.5$ (accreting pulsar with high magnetic field), and power law with photon index $\Gamma = 1.5$ (a black hole in hard state). All three models were further combined with a model of interstellar absorption (XSPEC phabs[6]) with two different absorption values (for a total of six models considered): 0.5×10^{22} cm^{-2} and 2.0×10^{22} cm^{-2}. The models and their parameters are also listed in Table 2. For these models, the main source of absorption is assumed to be the circumstellar material around the progenitor. Assuming a conservative average host galaxy extinction for CCSNe of $A_V \sim 1$ (Mattila et al. 2012) and converting this into a hydrogen column density according to the formula $N_{\rm H} = 1.79 \times 10^{21} A_V$ (Predehl & Schmitt 1995) results in a column density of 0.2×10^{22} cm^{-2}. This is significantly lower than the absorption values used in our models and we therefore do not consider the effects of host galaxy interstellar gas separately. The one exception to this is SN 2001ci, which has an unusually high A_V of ∼5–6 (Filippenko & Chornock 2001) corresponding to $N_{\rm H} \sim 1.0 \times 10^{22}$ cm^{-2}. We do not account for this higher extinction separately, but note that only the higher absorption models are realistic for this particular SN.

The data were processed using *Chandra's* CIAO 4.6 software package. In most cases, only a single observation existed of the given target. For these, prior to analysis, all of the data were reprocessed with the *chandra_repro* script to apply standard corrections (using CALDB version 4.6.1.1). In cases where multiple observations of the same area were available, these were first aligned with each other. In most cases, the relative astrometry of the original data was already sufficiently accurate that after reprocessing with *chandra_repro*, the data could simply be aligned with the *reproject_obs* tool. However, in some cases, it was beneficial to apply a correction into the aspect solution of the individual observations to ensure their coordinate grids were better aligned prior to reprojecting their tangent planes. In such cases, a wavelet analysis (with CIAO's *wavdetect* tool) was first applied to detect a number of sources in each observation. These sources were then matched on the individual observations (using CIAO's *reproject_aspect* script) to produce an aspect correction, which was then applied by reprocessing the data with *chandra_repro* before finishing the alignment process with *reproject_obs*.

After alignment and reprocessing, all data sets were divided into pre-explosion and post-explosion data for each SN. Combined photon-count maps and exposure maps were then made using CIAO's *flux_obs* tool for each SN in both categories. The exposure maps are in units of cm^2 s and combine instrument quantum efficiency with the exposure time as the telescope is dithered across the sky. They were calculated using spectral weights (produced with *make_instmap_weights*) for each of the six models. The energy range used for all models and maps was 0.5–7.0 keV.

For most targets, the flux was measured using a circular aperture with a radius of 2.5 arcsec at the known position of the SN (which contains more than 90 per cent of *Chandra's* PSF for sources less than 2 arcmin from the optical axis, see http://cxc.harvard.edu/proposer/POG/html/chap4.html, fig. 4.13). In cases where the

[6] The default values for cross-sections (xsect) and abundances (abund) were used, these being bcmc and angr, respectively.

Downloaded from http://mnras.oxfordjournals.org/ at University of Turku on February 1, 2016

Table 1. List of all sample SNe and available *Chandra* observations.

Name	*Chandra* observation ID[a]	Epoch[b]	Exposure pre-SN (ks)	Exposure post-SN (ks)
SN 1983I	859, 2148, 10403, 10404, 10775, 10776, 10777, 10778, 10779, 10780, 10781, 10782 10801, 10824	1983 Apr 25	–	444.6
SN 1983N	793, 2064, 12992, 12993, 12994, 12995, 12996, 13202, 13241, 13248, 14332, 14342	1983 July 15	–	791.3
SN 1983V	3554, 6868, 6869, 6870, 6871, 6872, 6873, 13920, 13921	1983 Dec 4	–	302.2
SN 1984L	7861	1984 Aug 20	–	5.1
SN 1985F	7147	1984 June 12	–	9.4
SN 1990U	10120, 11230	1990 Aug 2	–	35.4
SN 1991N	2939	1991 Apr 2	–	48.2
SN 1993J	735, 5600, 5601, 5935, 5936, 5937, 5938, 5939, 5940, 4941, 5942, 5943, 5944 5945, 5946, 5947, 5948, 5949, 6174, 6346, 6347, 6892, 6893, 6894, 6895, 6896 6897, 6898, 6899, 6900, 6901, 9122, 12301	1993 Mar 30	–	752.3
SN 1994I	354, 1622, 3932, 12562, 12668, 13812, 13813, 13814, 13815, 13816, 15496, 15553	1994 Apr 9	–	856.1
SN 1996D	15050	1996 Feb 9	–	16.0
SN 1996N	16350	1996 Mar 12	–	48.7
SN 1996aq	11229	1996 Aug 17	–	7.0
SN 1997X	4061	1997 Feb 1	–	10.8
SN 1998T	1641, 6227, 15077, 15619	1998 Mar 3	–	125.6
SN 1998bo	11505	1998 Apr 22	–	20.9
SN 1998bw	1956	1998 May 10	–	48.3
SN 1999dn	4800	1999 Aug 27	–	60.1
SN 1999eh	9104	1999 Oct 12	–	18.1
SN 1999ex	10392	1999 Nov 15	–	12.3
SN 2000cr	10395	2000 June 25	–	16.1
SN 2000ds	9528	2000 Oct 10	–	65.5
SN 2001ci	2038	2001 Apr 25[c]	26.9	–
SN 2001ig	3495, 3496	2001 Dec 10	–	47.9
SN 2002hf	2244	2002 Oct 29	9.2	–
SN 2003L	4417	2003 Jan 12	–	30.4
SN 2003bg	3870, 3871, 7605	2003 Mar 19	–	127.3
SN 2003is	16577	2003 Oct 14	–	9.8
SN 2004C	4659, 4660, 7607	2004 Jan 12	–	139.0
SN 2004dk	11226	2004 Aug 20	–	8.1
SN 2004gn	4017	2004 Dec 1	5.0	–
SN 2004gt	315, 3040, 3041, 3042, 3043, 3044, 3718	2004 Dec 12	425.2	–
SN 2005U	1641, 6227, 15077, 15619	2005 Jan 30	24.9	100.7
SN 2005at	15384	2005 Mar 5	–	52.8
SN 2005cz	6785	2005 July 17	–	15.2
SN 2006ep	7608, 9098	2006 Aug 30	–	8.0
SN 2007Y	15392, 16487	2007 Mar 3	–	49.7
SN 2007gr	387, 9579	2007 Aug 28	2.4	19.7
SN 2007ke	908, 11717, 12016, 12017, 12018	2007 Sept 24	48.5	135.5
SN 2007kj	6978, 8491	2007 Oct 2	46.3	–
SN 2008D	9104	2008 Jan 28[d]	–	18.1
SN 2008ax	1579, 4725, 4726	2008 Mar 22	98.9	–
SN 2008bo	9105, 10118	2008 Mar 31	–	19.4
SN 2009bb	10140	2009 Mar 21	–	10.0
SN 2009dt	10265	2009 Apr 28	5.1	–
SN 2009jf	10120, 11230	2009 Sept 27[e]	25.2	10.2
SN 2009mk	11236	2009 Dec 15	–	10.0
SN 2010O	1641, 6227, 15077, 15619	2010 Jan 24	35.2	90.4
SN 2011dh	354, 1622, 3932, 12562, 12668, 13812, 13813, 13814, 13815, 13816, 15496, 15553	2011 June 1	90.8	765.3
SN 2011ei	12669	2011 July 25	–	10.0
SN 2011hs	3947	2011 Nov 12	55.7	–
SN 2012ap	13785	2012 Feb 18	–	9.9
SN 2013ak	14795	2013 Mar 9	–	9.9
SN 2013dk	315, 3040, 3041, 3042, 3043, 3044, 3718	2013 June 22	425.2	–
SN 2013ff	11776	2013 Aug 31	30.1	–
SN 2013ge	16556	2013 Nov 8	–	18.8
SN 2014C	2198, 17569, 17570	2014 Jan 5	30.1	19.8
SN 2014L	7863	2014 Jan 26	5.1	–

Notes. [a]Only those *Chandra* OBSIDs are listed which were used for the measurements. [b]From Asiago Max. epoch: the date of optical maximum or discovery. [c]Explosion epoch narrowed down from Filippenko & Chornock (2001) to ensure the observation is correctly categorized. [d]Explosion epoch verified from Soderberg et al. (2008) to ensure the observation is correctly categorized. [e]Explosion epoch verified from Valenti et al. (2011) to ensure the observations are correctly categorized.

Downloaded from http://mnras.oxfordjournals.org/ at University of Turku on February 1, 2016

Table 2. Models used for the study.

Ref. no	Description	Model	Parameters	$\langle E_\gamma \rangle$ (keV)[a]	$C_{\rm abs}$ [b]
1	Soft-state black hole (low abs.)	Absorbed blackbody	$T = 1$ keV, $N_{\rm H} = 0.5 \times 10^{22}$ cm^{-2}	2.48	1.15
2	Soft-state black hole (high abs.)	Absorbed blackbody	$T = 1$ keV, $N_{\rm H} = 2.0 \times 10^{22}$ cm^{-2}	3.10	1.47
3	Accreting pulsar (low abs.)	Absorbed power law	$\Gamma = 0.5$, $N_{\rm H} = 0.5 \times 10^{22}$ cm^{-2}	2.81	1.11
4	Accreting pulsar (high abs.)	Absorbed power law	$\Gamma = 0.5$, $N_{\rm H} = 2.0 \times 10^{22}$ cm^{-2}	3.64	1.30
5	Hard-state black hole (low abs.)	Absorbed power law	$\Gamma = 1.5$, $N_{\rm H} = 0.5 \times 10^{22}$ cm^{-2}	2.00	1.35
6	Hard-state black hole (high abs.)	Absorbed power law	$\Gamma = 1.5$, $N_{\rm H} = 2.0 \times 10^{22}$ cm^{-2}	3.02	1.80

Notes. [a]Average photon energy for the model.
[b]Correction coefficient for absorption.

Table 3. SNe with pre-explosion *Chandra* X-ray data and measured photon counts.

Name	Host galaxy	SN type	Position[a]	Distance[b] (Mpc)	Aperture[c] (arcsec)	Counts (aperture)	Scaled background
SN 2001ci	NGC 3079	Ic	10:01:57.21+55:41:14.0[d]	18.1[e]	2.5/6	4	4.1
SN 2002hf	MCG-05-03-020	Ic	00:57:47.74−27:30:21.5[f]	77.5	3.5/9	10	9.3
SN 2004gn	NGC 4527	Ic	12:34:12.10+02:39:34.4[f]	14.2[g]	2.5/25	0	0.2
SN 2004gt	NGC 4038	Ic	12:01:50.42−18:52:13.5[h]	20.4[i]	2.5/12	694	206.4
SN 2005U	Arp 299	IIb	11:28:33.13+58:33:41.3[j]	48.2	2.5/6	15	11.1
SN 2007gr	NGC 1058	Ic	02:43:27.98+37:20:44.7[f]	9.3[k]	2.5/25	0	0.1
SN 2007ke	NGC 1129	Ib	02:54:23.90+41:34:16.3[f]	77.2	6.5/16	430	467.5
SN 2007kj	NGC 7803	Ib	00:01:19.58+13:06:30.6[f]	77.0	2.5/8	3	1.5
SN 2008ax	NGC 4490	IIb	12:30:40.80+41:38:14.5[f]	9.6[l]	2.5/7	8	8.2
SN 2009dt	IC 5169	Ic	22:10:09.27−36:05:42.6[f]	42.0	2.5/20	0	0.2
SN 2009jf	NGC 7479	Ib	23:04:52.98+12:19:59.5[f]	34.9	3/8	105	1.7
SN 2010O	Arp 299	Ib	11:28:33.86+58:33:51.6[f]	48.2	2.5/6	239	67.3
SN 2011dh	NGC 5194	IIb	13:30:05.11+47:10:10.9	7.8[m]	3/8	3	8.7
SN 2011hs	IC 5267	IIb	22:57:11.77−43:23:04.8	21.8	2.5/10	1	1.4
SN 2013dk	NGC 4038	Ic	12:01:52.72−18:52:18.3	20.4[i]	2.5/6	202	172.7
SN 2013ff	NGC 2748	Ic	09:13:38.88+76:28:10.8	24.8	2.5/8	1	2.6
SN 2014C	NGC 7331	Ib	22:37:05.60+34:24:31.9	15.1[g]	2.5/6	5	5.8
SN 2014L	NGC 4254	Ic	12:18:48.68+14:24:43.5	17.3[n]	2.5/10	1	1.1

Notes. [a]From Asiago if not indicated otherwise. [b]Distances that do not have a reference have been calculated from Hyperleda radial velocity corrected for the infall to the Virgo cluster (vvir) with $H_0 = 70$ km s^{-1}Mpc^{-1}. [c]Radius of source aperture/outer radius of background annulus. [d]Position confirmed from Van Dyk, Li & Filippenko (2003). [e]Average of values from Tully et al. (2009) and Springob et al. (2009). [f]Position confirmed from Unified Supernova Catalog (Lennarz et al. 2012). [g]Saha et al. (2006). [h]Position derived in this paper, see Section 4.1. [i]Fiorentino, Musella & Marconi (2013). [j]Position from Mattila, Monard & Li (2005, Li position). [k]Hunter et al. (2009). [l]Pastorello et al. (2008). [m]Ergon et al. (2014). [n]Average of values from Poznanski et al. (2009), Springob et al. (2009) and Russell (2002).

optical axis of one or more of the original individual observations was further than 2 arcmin from the SN position, the source aperture radius was increased accordingly (in increments of 0.5 arcsec) so that it contained at least 90 per cent of the PSF. Background was measured using an annulus around the source aperture circle, the size of which varied according to target. Generally the outer radius of the annulus was increased either to maintain roughly 2/5 ratio between the source aperture radius and the background annulus outer radius, or increased even further to ensure that at least 10 photons were located within the background area. For a list of the used source aperture and background annulus sizes, see Tables 3 and 4. Any unrelated sources were excluded from both the source apertures and the background annuli. For the purposes of this study, we conservatively consider a source unrelated if it is located further than ∼1.5 arcsec from the SN position or is not a point-source. For most pre-explosion targets there were no point-sources closer than 5 arcsec to the SN position. In all but two of the cases where more nearby point-sources existed, the position of the SN was known from literature with sufficient accuracy to rule out any association between such a source and the SN. The two exceptions, SN 2009jf and SN 2004gt, will be discussed in more detail in Section 4.1.

Background corrected flux was measured for each source aperture. If no source was found (within 3σ), then a 3σ upper limit was calculated instead using the number of detected counts inside the source aperture (equation 3 below). However, in many cases a short exposure time would result in the number of photons inside the aperture itself to be very low (or even zero), so in cases where there were no visible sources and the number of counts inside the source aperture was <20, we used Poissonian statistics to find the matching upper limit at a 99.87 per cent confidence level (corresponding to Gaussian 3σ; see e.g. Gehrels 1986), and calculated the 3σ upper limit using equation (4) below instead for these cases. To obtain unabsorbed flux, we calculated an absorption correction coefficient for each model by comparing the absorbed models with the corresponding unabsorbed model in XSPEC. The coefficients are listed in Table 2. Following Nielsen et al. (2012), for any 3σ detection we calculated the flux from

$$F = \frac{(n-b)\langle E_\gamma \rangle}{\zeta}, \quad (1)$$

where n is the number of photons from the source aperture, $\langle E_\gamma \rangle$ is average photon energy for the given model (see Table 2), ζ is the average value of the exposure map within the source aperture and b

Downloaded from http://mnras.oxfordjournals.org/ at University of Turku on February 1, 2016

Table 4. SNe with post-explosion *Chandra* X-ray data and measured photon counts.

Name	Host galaxy	SN type	Position[a]	Distance[b] (Mpc)	Aperture[c] (arcsec)	Counts (aperture)	Scaled background
SN 1983I	NGC 4051	Ic	12:03:11.77+44:31:00.6	13.7[d]	2.5/8	17	17.5
SN 1983N	NGC 5236	Ib	13:36:51.24−29:54:02.7[e]	4.6[f]	5/13	301	264.7
SN 1983V	NGC 1365	Ic	03:33:31.63−36:08:55.0[e]	19.6[f]	2.5/6	16	12.3
SN 1984L	NGC 991	Ib	02:35:30.52−07:09:30.5	20.4	2.5/20	0	0.2
SN 1985F	NGC 4618	Ib	12:41:33.01+41:09:05.9[e]	7.9[g]	2.5/15	1	0.4
SN 1990U	NGC 7479	Ib	23:04:54.92+12:18:20.1[e]	34.9	2.5/8	3	3.2
SN 1991N	NGC 3310	Ic	10:38:46.37+53:30:04.7[e]	17.5[h]	2.5/6	162	117.5
SN 1993J	NGC 3031	IIb	09:55:24.77+69:01:13.7[i]	3.6[j]	3/8	9498	60.2
SN 1994I	NGC 5194	Ic	13:29:54.12+47:11:30.4[k]	7.8[l]	3/8	362	200.9
SN 1996D	NGC 1614	Ic	04:34:00.30−08:34:44.0	66.4	2.5/6	27	15.3
SN 1996N	NGC 1398	Ib	03:38:55.31−26:20:04.1[e]	17.2	2.5/10	0	1.0
SN 1996aq	NGC 5584	Ic	14:22:22.72−00:23:23.8[e]	22.0[m]	2.5/20	1	0.3
SN 1997X	NGC 4691	Ib	12:48:14.28−03:19:58.5	16.4	2.5/6	1	7.1
SN 1998T	Arp 299	Ib	11:28:33.16+58:33:43.7[e]	48.2	2.5/6	603	216.1
SN 1998bo	ESO185-031	Ic	19:57:22.55−55:08:18.4[e]	67.4	10/30	12	9.8
SN 1998bw	E184-G82	Ic	19:35:03.31−52:50:44.6[n]	33.8	2.5/6	83	4.3
SN 1999dn	NGC 7714	Ib	23:36:14.81+02:09:08.4[o]	40.0	2.5/6	8	7.7
SN 1999eh	NGC 2770	Ib	09:09:32.67+33:07:16.9[e]	29.5	2.5/10	1	0.7
SN 1999ex	IC 5179	Ib	22:16:07.27−36:50:53.7[e]	46.3[p]	2.5/12	3	1.0
SN 2000cr	NGC 5395	Ic	13:58:38.37+37:26:12.9[e]	52.7	2.5/8	0	1.7
SN 2000ds	NGC 2768	Ib	09:11:36.28+60:01:43.3[q]	23.2	2.5/6	8	4.1
SN 2001ig	NGC 7424	IIb	22:57:30.69−41:02:25.9[e]	10.8[r]	2.5/7	38	1.1
SN 2003L	NGC 3506	Ic	11:03:12.33+11:04:38.3[e]	92.2	2.5/6	43	6.2
SN 2003bg	M-05-10-15	Ic	04:10:59.42−31:24:50.3[e]	16.3	2.5/7	632	7.1
SN 2003is	MCG+07-40-03	Ic	19:21:08.00+43:19:35.4[e]	81.9	5/22	0	0.9
SN 2004C	NGC 3683	Ic	11:27:29.72+56:52:48.2[e]	27.8	2.5/6	136	30.3
SN 2004dk	NGC 6118	Ib	16:21:48.93−02:16:17.3[e]	23.5	2.5/12	7	0.6
SN 2005U	Arp 299	IIb	11:28:33.13+58:33:41.3[s]	48.2	2.5/6	90	53.4
SN 2005at	NGC 6744	Ic	19:09:53.57−63:49:22.8[e]	9.0	2.5/10	1	0.8
SN 2005cz	NGC 4589	Ib	12:37:27.85+74:11:24.5[e]	32.6	2.5/8	0	1.6
SN 2006ep	NGC 0214	Ib	00:41:24.88+25:29:46.7[e]	66.1	2.5/15	0	0.3
SN 2007Y	NGC 1187	Ib	03:02:35.92−22:53:50.1[e]	17.3	3.5/10	4	1.7
SN 2007gr	NGC 1058	Ic	02:43:27.98+37:20:44.7[e]	9.3[t]	2.5/25	3	0.5
SN 2007ke	NGC 1129	Ib	02:54:23.90+41:34:16.3[e]	77.2	6.5/16	1182	1215.6
SN 2008D	NGC 2770	Ib	09:09:30.65+33:08:20.3[e]	29.5	2.5/10	11	0.7
SN 2008bo	NGC 6643	IIb	18:19:54.41+74:34:21.0	25.4	2.5/8	1	0.8
SN 2009bb	NGC 3278	Ic	10:31:33.88−39:57:30.0[u]	40.0	2.5/8	10	1.7
SN 2009jf	NGC 7479	Ib	23:04:52.98+12:19:59.5[e]	34.9	3/8	76	1.5
SN 2009mk	E293-G34	IIb	00:06:21.37−41:28:59.8[e]	18.7	2.5/15	2	0.5
SN 2010O	Arp 299	Ib	11:28:33.86+58:33:51.6[e]	48.2	2.5/6	759	244.3
SN 2011dh	NGC 5194	IIb	13:30:05.11+47:10:10.9	7.8[l]	3/8	1193	49.1
SN 2011ei	NGC 6925	IIb	20:34:22.62−31:58:23.6	38.3	2.5/8	1	1.3
SN 2012ap	NGC 1729	Ic	05:00:13.72−03:20:51.2	50.5	2.5/20	2	0.3
SN 2013ak	E430-G20	IIb	08:07:06.69−28:03:10.1	11.6[v]	2.5/15	30	0.4
SN 2013ge	NGC 3287	Ic	10:34:48.46+21:39:41.9	19.7	2.5/12	0	0.5
SN 2014C	NGC 7331	Ib	22:37:05.60+34:24:31.9	15.1	2.5/6	515	6.0

Notes. [a]From Asiago if not indicated otherwise. [b]Distances that do not have a reference have been calculated from Hyperleda radial velocity corrected for the infall to the Virgo cluster (vvir) with $H_0 = 70$ km s^{-1}Mpc^{-1}. [c]Radius of source aperture/outer radius of background annulus. [d]Average of values from Tully et al. (2009), Nasonova, de Freitas Pacheco & Karachentsev (2011), Pounds & King (2013), Russell (2002). [e]Position confirmed from Unified Supernova Catalog (Lennarz et al. 2012). [f]Saha et al. (2006). [g]Karachentsev, Makarov & Kaisina (2013). [h]Terry, Paturel & Ekholm (2002). [i]Position from Marcaide et al. (1993). [j]Gerke et al. (2011). [k]Position from Rupen et al. (1994). [l]Ergon et al. (2014). [m]Fiorentino et al. (2013). [n]Position from Dominici et al. (1998). [o]Position confirmed from Van Dyk et al. (2003). [p]Average of values from Wood-Vasey et al. (2008), Mandel, Narayan & Kirshner (2011), Mandel et al. (2009), Wang et al. (2006), Takanashi, Doi & Yasuda (2008), Ganeshalingam, Li & Filippenko (2013), Weyant et al. (2014), Hicken et al. (2009), Prieto, Rest & Suntzeff (2006), Jha, Riess & Kirshner (2007) and Reindl et al. (2005). [q]Position obtained from Unified Supernova Catalog (Lennarz et al. 2012). [r]Mattila et al. (2012). [s]Position from Mattila et al. (2005). [t]Hunter et al. (2009). [u]Position confirmed from Bietenholz et al. (2010). [v]Average value from Theureau et al. (2007).

is scaled background, the number of background counts $n_{\rm bg}$ scaled to the size of the source aperture:

$$b = \frac{n_{\rm bg} \times A_{\rm src}}{A_{\rm bg}}, \quad (2)$$

where $A_{\rm src}$ and $A_{\rm bg}$ are the surface areas of the source and background regions, respectively. The flux upper limit was calculated from

$$F_{\rm UL} = \frac{3\sqrt{n}\langle E_\gamma \rangle}{\zeta} \quad (3)$$

Downloaded from http://mnras.oxfordjournals.org/ at University of Turku on February 1, 2016

for high photon count cases. For the low photon count cases, the flux upper limit was instead calculated from

$$F_{\rm UL} = \frac{(\mu - b)\langle E_\gamma \rangle}{\zeta}, \quad (4)$$

where μ is the 0.9987 confidence level Poissonian upper limit corresponding to the number of photons within the source aperture, according to Gehrels (1986). Finally, the unabsorbed luminosity for each F and $F_{\rm UL}$ was calculated from

$$L = 4\pi C_{\rm abs} F d^2, \quad (5)$$

where $C_{\rm abs}$ is the correction coefficient for absorption and d is the distance to the host galaxy. The distances used for calculating the luminosities were obtained via NED[7] (see Tables 3 and 4 for details), or calculated from the Hyperleda[8] radial velocity corrected for infall on to the Virgo cluster (vvir) using $H_0 = 70$ km s^{-1}Mpc^{-1}.

4 RESULTS

Basic information about each SN (host galaxy, SN type, position, distance), as well as non-model-specific results of our measurements are presented in Table 3 for those SNe with pre-explosion data, and in Table 4 for those with post-explosion data. Targets with both types of data are present in both. The model-specific results – average exposure map values and luminosity upper limits – are presented in Table 5 and Tables 6 and 7 for pre- and post-explosion data, respectively. Any measured luminosities for sources that have a flux above the 3σ detection threshold and their errors are also included in these tables. The models are numbered according to Table 2.

4.1 Detected pre-explosion sources

Although for most pre-explosion targets no source flux above the 3σ detection threshold was found, there are three targets that do display a clear signal: SN 2004gt, SN 2009jf and SN 2010O.

In the case of SN 2004gt, a complex emission area permeates the entire source region, confusing any signal from a potential progenitor (see Fig. 1). Because this emission is primarily from low-energy photons, we re-examined this data set using a higher, 1.5–8.0 keV energy range. First, we corrected the aspect solution of the seven original *Chandra* observations using CIAO's *reproject_aspect* tool by matching sources found with *wavdetect* with the USNO A2.0 catalog (Monet 1998), then reprocessing the data the same way as discussed before. We then remade the photon count and exposure maps for SN 2004gt position using the higher 1.5–8.0 keV energy range. The corrected count map was convolved with a Gaussian kernel with $\sigma = 1.27$ pixels (FWHM = 1.5 arcsec) to enhance the detection of faint point sources. In the convolved image a point-like source becomes visible close to the position of SN 2004gt. We identify this source as the known X-ray source CXOU J120150.4−185212 (Zezas et al. 2006). To determine whether this pre-explosion source is coincident with the SN position, we determined its centre coordinates with one-dimensional Gaussian fitting using the IRAF XIMTOOL package and with centroiding and Gaussian fitting as implemented in the IRAF APPHOT package. These three methods gave similar coordinates with a standard deviation of 0.4 pixels. However, the uncertainty in the centre coordinates is probably larger than this given the low S/N of the object in the original unconvolved data and we therefore adopt 1 pixel (corresponding to 0.5 arcsec) as the uncertainty in its (x,y) position. Combining this error with the uncertainty in the absolute astrometric calibration yields a total error of ±0.6 arcsec for both the RA and Dec of the pre-explosion source (at the distance of SN 2004gt, 1 arcsec corresponds to a projected distance of ∼100 pc). We therefore adopt the position RA = $12^{\rm h}01^{\rm m}50\overset{\rm s}{.}40$, Dec = $-18^\circ52'12\overset{''}{.}7$ for the source.

We also derived new absolute astrometry for SN 2004gt making use of near-infrared *K*s-band imaging of NGC 4038/9 obtained as a part of a search for SNe in the nuclear regions of starburst galaxies (see Mattila, Meikle & Greimel 2004) with the William Herschel Telescope LIRIS instrument on 2005 January 30 and INGRID instrument on 2002 January 3. The images were reduced using standard procedures in IRAF (see Kangas et al. 2013). For this the World Coordinate System (WCS) of the LIRIS image was calibrated making use of the centroid positions of 26 point-like sources (incl. both foreground stars and star clusters in NGC 4038/9) together with their coordinates from the 2MASS catalogue (Skrutskie et al., 2006). The SN is located in proximity of a bright star cluster making the precise determination of its location in ground-based seeing limited images more difficult. To obtain accurate coordinates for the SN, we therefore aligned the pre-explosion INGRID image to the LIRIS image and performed image subtraction using the ISIS 2.2 package (Alard & Lupton 1998; Alard 2000). The centroid position of the SN measured from the subtracted image corresponds to RA = $12^{\rm h}01^{\rm m}50\overset{\rm s}{.}42$, Dec = $-18^\circ52'13\overset{''}{.}5$, with uncertainty of 0.16 arcsec in RA and 0.19 arcsec in Dec dominated by the uncertainty in the WCS transformation. The SN is therefore coincident with the derived position of the source within $\sim 1\sigma$.

We measured the flux of this source in the higher energy range, and found 50 photons inside a source aperture with a 2.5 arcsec radius. A scaled background of 25 photons was obtained from an annulus with outer radius of 12 arcsec centred on the source (excluding two interfering sources from the background, see Fig. 1). The number of photons was too low to obtain a spectrum, and we therefore measured the luminosity using the same models we used for the other SNe.[9] Rescaling from 1.5–8.0 keV to the 0.5–7.0 keV energy range, we obtained the unabsorbed luminosity of $(3.7 \pm 1.1) \times 10^{37}$ erg s^{-1} for the low-absorption 1 keV temperature blackbody (model 1), $(5.8 \pm 1.6) \times 10^{37}$ erg s^{-1} for the high-absorption 0.5 photon-index power law (model 4), with the luminosities for other models falling between these two values. The average luminosity from all models is 4.6×10^{37} erg s^{-1}. We note that this constitutes a detection with an approximately 3σ significance. Note that the values presented in Table 5 are the measurements for the original 0.5–7.0 keV energy range at the SN position using the extraction regions depicted in Fig. 1. Because the emission in this energy range most likely originates from the diffuse emission field permeating the region, these measurements do not accurately reflect the nature of the source discussed above, although it is contained within the source aperture. We also note the proximity of a bright star cluster approximately 1 arcsec north and 0.6 arcsec west from the SN position (see fig. 1 in Maund, Smartt & Schweizer 2005), possibly contributing some X-ray sources/emission to the vicinity of the SN location (see e.g. Poutanen et al. 2013, for possible associations between star clusters and HMXBs).

[7] http://ned.ipac.caltech.edu/

[8] Paturel et al. (2003): See http://atlas.obs-hp.fr/hyperleda/.

[9] The average photon energies and absorption correction factors were scaled accordingly for the 1.5–8.0 keV energy range, with other parameters being the same as in Table 2.

Downloaded from http://mnras.oxfordjournals.org/ at University of Turku on February 1, 2016

Table 5. X-ray luminosities and upper limits of X-ray luminosity (pre-explosion).

	(1) Soft-state BH (low abs.)		(2) Soft-state BH (high abs.)		(3) Accr. pulsar (low abs.)	
Name	Exp. map av. value (cm^2s)	Luminosity (erg s^{-1})	Exp. map av. value (cm^2s)	Luminosity (erg s^{-1})	Exp. map av. value (cm^2s)	Luminosity (erg s^{-1})
2001ci[a]	1.17×10^7	$<1.6 \times 10^{38}$	1.06×10^7	$<2.8 \times 10^{38}$	1.04×10^7	$<1.9 \times 10^{38}$
2002hf	3.83×10^6	$<1.2 \times 10^{40}$	3.48×10^6	$<2.2 \times 10^{40}$	3.41×10^6	$<1.5 \times 10^{40}$
2004gn	2.12×10^6	$<3.3 \times 10^{38}$	1.93×10^6	$<5.8 \times 10^{38}$	1.89×10^6	$<4.1 \times 10^{38}$
2004gt[b]	1.80×10^8	$(6.1\pm0.3) \times 10^{38}$	1.64×10^8	$(10.8\pm0.6) \times 10^{38}$	1.61×10^8	$(7.6\pm0.4) \times 10^{38}$
2005U	7.25×10^6	$<3.4 \times 10^{39}$	6.86×10^6	$<5.8 \times 10^{39}$	6.72×10^6	$<4.1 \times 10^{39}$
2007gr	9.29×10^5	$<3.3 \times 10^{38}$	8.32×10^5	$<5.9 \times 10^{38}$	8.24×10^5	$<4.1 \times 10^{38}$
2007ke	1.57×10^7	$<1.3 \times 10^{40}$	1.48×10^7	$<2.2 \times 10^{40}$	1.44×10^7	$<1.5 \times 10^{40}$
2007kj	1.37×10^7	$<2.6 \times 10^{39}$	1.31×10^7	$<4.4 \times 10^{39}$	1.27×10^7	$<3.1 \times 10^{39}$
2008ax	4.15×10^7	$<1.5 \times 10^{37}$	3.78×10^7	$<2.7 \times 10^{37}$	3.69×10^7	$<1.9 \times 10^{37}$
2009dt	1.76×10^6	$<3.5 \times 10^{39}$	1.69×10^6	$<5.9 \times 10^{39}$	1.63×10^6	$<4.2 \times 10^{39}$
2009jf	1.03×10^7	$(6.7\pm0.7) \times 10^{39}$	9.40×10^6	$(1.2\pm0.1) \times 10^{40}$	9.12×10^6	$(8.3\pm0.8) \times 10^{39}$
2010O[c]	1.09×10^7	$(2.0\pm0.2) \times 10^{40}$	1.01×10^7	$(3.4\pm0.3) \times 10^{40}$	9.90×10^6	$(2.4\pm0.2) \times 10^{40}$
2011dh	3.78×10^7	$<3.5 \times 10^{36}$	3.44×10^7	$<6.1 \times 10^{36}$	3.37×10^7	$<4.3 \times 10^{36}$
2011hs	2.27×10^7	$<8.6 \times 10^{37}$	2.07×10^7	$<1.5 \times 10^{38}$	2.02×10^7	$<1.1 \times 10^{38}$
2013dk	1.79×10^8	$<5.4 \times 10^{37}$	1.62×10^8	$<9.6 \times 10^{37}$	1.59×10^8	$<6.7 \times 10^{37}$
2013ff	1.24×10^7	$<1.7 \times 10^{38}$	1.14×10^7	$<3.0 \times 10^{38}$	1.11×10^7	$<2.1 \times 10^{38}$
2014C	1.30×10^7	$<9.8 \times 10^{37}$	1.18×10^7	$<1.7 \times 10^{38}$	1.16×10^7	$<1.2 \times 10^{38}$
2014L	2.06×10^6	$<6.2 \times 10^{38}$	1.89×10^6	$<1.1 \times 10^{39}$	1.84×10^6	$<7.6 \times 10^{38}$

	(4) Accr. pulsar (high abs.)		(5) Hard-state BH (low abs.)		(6) Hard-state BH (high abs.)	
Name	Exp. map av. value (cm^2s)	Luminosity (erg s^{-1})	Exp. map av. value (cm^2s)	Luminosity (erg s^{-1})	Exp. map av. value (cm^2s)	Luminosity (erg s^{-1})
2001ci[a]	9.23×10^6	$<3.3 \times 10^{38}$	1.23×10^7	$<1.4 \times 10^{38}$	1.05×10^7	$<3.4 \times 10^{38}$
2002hf	3.04×10^6	$<2.6 \times 10^{40}$	3.99×10^6	$<1.1 \times 10^{40}$	3.44×10^6	$<2.6 \times 10^{40}$
2004gn	1.69×10^6	$<6.9 \times 10^{38}$	2.20×10^6	$<3.0 \times 10^{38}$	1.91×10^6	$<7.0 \times 10^{38}$
2004gt[b]	1.43×10^8	$(12.9\pm0.7) \times 10^{38}$	1.89×10^8	$(5.6\pm0.3) \times 10^{38}$	1.62×10^8	$(13.1\pm0.7) \times 10^{38}$
2005U	6.30×10^6	$<6.6 \times 10^{39}$	7.32×10^6	$<3.2 \times 10^{39}$	6.78×10^6	$<7.0 \times 10^{39}$
2007gr	7.24×10^5	$<7.0 \times 10^{38}$	9.86×10^5	$<2.9 \times 10^{38}$	8.25×10^5	$<7.1 \times 10^{38}$
2007ke	1.34×10^7	$<2.5 \times 10^{40}$	1.59×10^7	$<1.2 \times 10^{40}$	1.46×10^7	$<2.7 \times 10^{40}$
2007kj	1.21×10^7	$<5.0 \times 10^{39}$	1.36×10^7	$<2.5 \times 10^{39}$	1.29×10^7	$<5.3 \times 10^{39}$
2008ax	3.30×10^7	$<3.2 \times 10^{37}$	4.30×10^7	$<1.4 \times 10^{37}$	3.73×10^7	$<3.2 \times 10^{37}$
2009dt	1.55×10^6	$<6.6 \times 10^{39}$	1.74×10^6	$<3.4 \times 10^{39}$	1.66×10^6	$<7.1 \times 10^{39}$
2009jf	8.20×10^6	$(1.4\pm0.1) \times 10^{40}$	1.05×10^7	$(6.2\pm0.6) \times 10^{39}$	9.27×10^6	$(1.4\pm0.1) \times 10^{40}$
2010O[c]	9.13×10^6	$(4.0\pm0.4) \times 10^{40}$	1.11×10^7	$(1.9\pm0.2) \times 10^{40}$	1.00×10^7	$(4.2\pm0.4) \times 10^{40}$
2011dh	3.01×10^7	$<7.2 \times 10^{36}$	3.93×10^7	$<3.2 \times 10^{36}$	3.40×10^7	$<7.4 \times 10^{36}$
2011hs	1.81×10^7	$<1.8 \times 10^{38}$	2.35×10^7	$<7.9 \times 10^{37}$	2.04×10^7	$<1.8 \times 10^{38}$
2013dk	1.42×10^8	$<1.1 \times 10^{38}$	1.87×10^8	$<4.9 \times 10^{37}$	1.60×10^8	$<1.2 \times 10^{38}$
2013ff	1.00×10^7	$<3.5 \times 10^{38}$	1.27×10^7	$<1.6 \times 10^{38}$	1.13×10^7	$<3.6 \times 10^{38}$
2014C	1.03×10^7	$<2.1 \times 10^{38}$	1.37×10^7	$<8.9 \times 10^{37}$	1.17×10^7	$<2.1 \times 10^{38}$
2014L	1.66×10^6	$<1.3 \times 10^{39}$	2.12×10^6	$<5.7 \times 10^{38}$	1.87×10^6	$<1.3 \times 10^{39}$

Notes. [a]SN 2001ci has an unusually high host galaxy absorption which has not been corrected for here. Therefore, only the higher absorption models (2, 4 and 6) should be considered realistic. [b]The luminosities presented here for SN 2004gt are the source aperture luminosities for the original 0.5–7.0 keV energy range and do not reflect the properties of the source discussed in Section 4.1. [c]The luminosities presented here for SN 2010O are a combination of multiple different sources found inside the source aperture and do not represent any particular single source, see Section 4.1.

In the case of SN 2009jf the flux is from the ULX CXOU J230453.0+121959, which overlaps with the SN position and could potentially be associated with the SN, although this cannot be confirmed (Voss et al. 2011). The post-explosion observation, taken ∼30 d after the SN explosion (2009 September 23, from Valenti et al. 2011), shows the ULX with a substantially increased luminosity ($L_{\rm diff} \sim 4.3 \times 10^{39}$ erg s^{-1}). As Voss et al. (2011) also note, this would be consistent with the increase in the flux being caused by the SN.

SN 2010O in the galaxy Arp 299 has an extremely complex background, which makes any measurements taken for this source difficult. Nelemans et al. (2010) suggested the detection of a progenitor for SN 2010O by measuring the X-ray flux variability between the two *Chandra* pre-explosion data sets (OBSIDs 1641 and 6227). We had, in addition to these, two more recent post-explosion data sets (OBSIDs 15077 and 15619). We subtracted the combined (exposure-corrected) pre- and post-explosion observations from each other to see how much variability there was in the source aperture area (see Fig. 2 for the exposure-corrected difference map). While there is variability within the source aperture, it is widely distributed spatially and could not be attributed to any single point source (notably, SN 2010O cannot be clearly identified from the post-explosion data set). This suggests the area contains multiple overlapping variable sources within a very complex X-ray background, and identifying any particular sources inside the source aperture could not be made with any confidence. We have included the measured luminosities for this SN in our sample for completeness but note that the results presented here cannot be associated with a progenitor but rather reflect the complex nature of the extraction area. The post-explosion measurements of SN 2010O

Downloaded from http://mnras.oxfordjournals.org/ at University of Turku on February 1, 2016

Table 6. X-ray luminosities and upper limits of X-ray luminosity (post-explosion, part 1).

Name	(1) Soft-state BH (low abs.)		(2) Soft-state BH (high abs.)		(3) Accr. pulsar (low abs.)	
	Exp. map av. value ($cm^2 s$)	Luminosity ($erg\ s^{-1}$)	Exp. map av. value ($cm^2 s$)	Luminosity ($erg\ s^{-1}$)	Exp. map av. value ($cm^2 s$)	Luminosity ($erg\ s^{-1}$)
1983I	5.69×10^7	$<2.9 \times 10^{37}$	5.91×10^7	$<4.5 \times 10^{37}$	5.67×10^7	$<3.2 \times 10^{37}$
1983N	3.08×10^8	$<2.0 \times 10^{36}$	2.83×10^8	$<3.4 \times 10^{36}$	2.73×10^8	$<2.4 \times 10^{36}$
1983V	6.22×10^7	$<6.7 \times 10^{37}$	6.08×10^7	$<1.1 \times 10^{38}$	5.86×10^7	$<7.7 \times 10^{37}$
1984L	2.15×10^6	$<6.8 \times 10^{38}$	1.97×10^6	$<1.2 \times 10^{39}$	1.91×10^6	$<8.4 \times 10^{38}$
1985F	3.97×10^6	$<7.3 \times 10^{37}$	3.64×10^6	$<1.3 \times 10^{38}$	3.54×10^6	$<9.0 \times 10^{37}$
1990U	1.43×10^7	$<4.4 \times 10^{38}$	1.31×10^7	$<7.7 \times 10^{38}$	1.27×10^7	$<5.4 \times 10^{38}$
1991N	2.04×10^7	$(3.7\pm1.0) \times 10^{38}$	1.85×10^7	$(6.4\pm1.8) \times 10^{38}$	1.81×10^7	$(4.5\pm1.3) \times 10^{38}$
1993J	1.50×10^8	$(45.3\pm0.5) \times 10^{37}$	1.46×10^8	$(74.5\pm0.8) \times 10^{37}$	1.41×10^8	$(52.7\pm0.5) \times 10^{37}$
1994I	3.46×10^8	$(1.6\pm0.2) \times 10^{37}$	3.20×10^8	$(2.7\pm0.3) \times 10^{37}$	3.08×10^8	$(1.9\pm0.2) \times 10^{37}$
1996D	6.45×10^6	$<5.8 \times 10^{39}$	5.99×10^6	$<1.0 \times 10^{40}$	5.75×10^6	$<7.1 \times 10^{39}$
1996N	1.64×10^7	$<5.5 \times 10^{37}$	1.60×10^7	$<9.0 \times 10^{37}$	1.53×10^7	$<6.5 \times 10^{37}$
1996aq	2.95×10^6	$<7.7 \times 10^{38}$	2.71×10^6	$<1.3 \times 10^{39}$	2.63×10^6	$<9.4 \times 10^{38}$
1997X	4.12×10^6	$<6.3 \times 10^{37}$	3.75×10^6	$<1.1 \times 10^{38}$	3.67×10^6	$<7.8 \times 10^{37}$
1998T	4.89×10^7	$(10.1\pm0.6) \times 10^{39}$	4.55×10^7	$(1.7\pm0.1) \times 10^{40}$	4.38×10^7	$(12.3\pm0.8) \times 10^{39}$
1998bo	5.93×10^6	$<7.0 \times 10^{39}$	5.64×10^6	$<1.2 \times 10^{40}$	5.41×10^6	$<8.4 \times 10^{39}$
1998bw	2.09×10^7	$(2.4\pm0.3) \times 10^{39}$	1.89×10^7	$(4.1\pm0.5) \times 10^{39}$	1.86×10^7	$(2.9\pm0.3) \times 10^{39}$
1999dn	2.40×10^7	$<4.7 \times 10^{38}$	2.19×10^7	$<8.3 \times 10^{38}$	2.14×10^7	$<5.8 \times 10^{38}$
1999eh	7.38×10^6	$<5.3 \times 10^{38}$	6.76×10^6	$<9.2 \times 10^{38}$	6.56×10^6	$<6.5 \times 10^{38}$
1999ex	4.83×10^6	$<2.8 \times 10^{39}$	4.44×10^6	$<4.9 \times 10^{39}$	4.30×10^6	$<3.5 \times 10^{39}$
2000cr	6.63×10^6	$<1.1 \times 10^{39}$	6.09×10^6	$<2.0 \times 10^{39}$	5.90×10^6	$<1.4 \times 10^{39}$
2000ds	2.71×10^7	$<1.8 \times 10^{38}$	2.48×10^7	$<3.1 \times 10^{38}$	2.41×10^7	$<2.2 \times 10^{38}$
2001ig	2.06×10^7	$(1.1\pm0.2) \times 10^{38}$	1.87×10^7	$(2.0\pm0.3) \times 10^{38}$	1.83×10^7	$(1.4\pm0.2) \times 10^{38}$
2003L	1.30×10^7	$(1.3\pm0.2) \times 10^{40}$	1.18×10^7	$(2.3\pm0.4) \times 10^{40}$	1.16×10^7	$(1.6\pm0.3) \times 10^{40}$
2003bg	5.39×10^7	$(16.9\pm0.7) \times 10^{38}$	4.92×10^7	$(3.0\pm0.1) \times 10^{39}$	4.80×10^7	$(20.7\pm0.8) \times 10^{38}$
2003is	2.96×10^6	$<7.0 \times 10^{39}$	2.86×10^6	$<1.2 \times 10^{40}$	2.65×10^6	$<8.6 \times 10^{39}$
2004C	5.81×10^7	$(7.7\pm0.8) \times 10^{38}$	5.32×10^7	$(1.3\pm0.1) \times 10^{39}$	5.18×10^7	$(9.4\pm1.0) \times 10^{38}$
2004dk	3.41×10^6	$(5.7^{+3.3}_{-2.3}) \times 10^{38}$	3.14×10^6	$(9.9^{+5.8}_{-4.0}) \times 10^{38}$	3.04×10^6	$(7.0^{+4.1}_{-2.8}) \times 10^{38}$
2005U	4.15×10^7	$(1.1\pm0.3) \times 10^{39}$	3.85×10^7	$(1.9\pm0.5) \times 10^{39}$	3.70×10^7	$(1.4\pm0.4) \times 10^{39}$
2005at	1.76×10^7	$<2.0 \times 10^{37}$	1.72×10^7	$<3.3 \times 10^{37}$	1.65×10^7	$<2.4 \times 10^{37}$
2005cz	5.86×10^6	$<5.0 \times 10^{38}$	5.37×10^6	$<8.7 \times 10^{38}$	5.22×10^6	$<6.1 \times 10^{38}$
2006ep	3.40×10^6	$<4.4 \times 10^{39}$	3.12×10^6	$<7.7 \times 10^{39}$	3.03×10^6	$<5.5 \times 10^{39}$
2007Y	1.65×10^7	$<1.3 \times 10^{38}$	1.61×10^7	$<2.1 \times 10^{38}$	1.54×10^7	$<1.5 \times 10^{38}$
2007gr	6.78×10^6	$<8.5 \times 10^{37}$	6.50×10^6	$<1.4 \times 10^{38}$	6.31×10^6	$<1.0 \times 10^{38}$
2007ke	4.51×10^7	$<7.5 \times 10^{39}$	4.32×10^7	$<1.2 \times 10^{40}$	4.18×10^7	$<8.8 \times 10^{39}$
2008D	7.52×10^6	$(6.5^{+2.8}_{-2.1}) \times 10^{38}$	6.90×10^6	$(1.1^{+0.5}_{-0.4}) \times 10^{39}$	6.69×10^6	$(8.0^{+3.4}_{-2.5}) \times 10^{38}$
2008bo	8.16×10^6	$<3.5 \times 10^{38}$	7.50×10^6	$<6.1 \times 10^{38}$	7.27×10^6	$<4.3 \times 10^{38}$
2009bb	4.21×10^6	$(1.7^{+0.9}_{-0.6}) \times 10^{39}$	3.87×10^6	$(3.0^{+1.5}_{-1.1}) \times 10^{39}$	3.76×10^6	$(2.1^{+1.1}_{-0.8}) \times 10^{39}$
2009jf	4.26×10^6	$(1.2\pm0.1) \times 10^{40}$	3.92×10^6	$(2.0\pm0.2) \times 10^{40}$	3.80×10^6	$(1.4\pm0.2) \times 10^{40}$
2009mk	4.20×10^6	$<4.7 \times 10^{38}$	3.87×10^6	$<8.1 \times 10^{38}$	3.75×10^6	$<5.8 \times 10^{38}$
2010O	3.72×10^7	$(17.6\pm0.9) \times 10^{39}$	3.46×10^7	$(3.0\pm0.2) \times 10^{40}$	3.32×10^7	$(2.2\pm0.1) \times 10^{40}$
2011dh	3.14×10^8	$(12.1\pm0.4) \times 10^{37}$	2.91×10^8	$(20.1\pm0.6) \times 10^{37}$	2.80×10^8	$(14.9\pm0.4) \times 10^{37}$
2011ei	4.12×10^6	$<1.5 \times 10^{39}$	3.81×10^6	$<2.6 \times 10^{39}$	3.67×10^6	$<1.8 \times 10^{39}$
2012ap	4.11×10^6	$<3.6 \times 10^{39}$	3.80×10^6	$<6.2 \times 10^{39}$	3.66×10^6	$<4.4 \times 10^{39}$
2013ak	4.08×10^6	$(5.4\pm1.0) \times 10^{38}$	3.80×10^6	$(9.2\pm1.7) \times 10^{38}$	3.64×10^6	$(6.6\pm1.2) \times 10^{38}$
2013ge	7.66×10^6	$<1.7 \times 10^{38}$	7.13×10^6	$<2.9 \times 10^{38}$	6.83×10^6	$<2.1 \times 10^{38}$
2014C	7.95×10^6	$(8.0\pm0.4) \times 10^{39}$	7.48×10^6	$(13.5\pm0.6) \times 10^{39}$	7.11×10^6	$(9.8\pm0.4) \times 10^{39}$

Note that the luminosities presented here do not accurately reflect the luminosity of SNe due to chosen spectral models or multi-epoch stacking of observations.

likewise reflect the complexity of the region, rather than any clear source that could be associated with the SN.

4.2 Detected post-explosion sources

In the post-explosion observations, in addition to SN 2009jf and SN 2010O, there are 16 other sources that have flux above the 3σ detection threshold. Of these, in the cases of SN 1993J (Chandra et al. 2009), SN 1998bw (Kouveliotou et al. 2004), SN 2001ig (Schlegel & Ryder 2002), SN 2003L (Soderberg et al. 2005), 2003bg (Pooley & Lewin 2003), SN 2004C (Perna et al. 2008), SN 2008D (Soderberg et al. 2008), SN 2011dh (Maeda et al. 2014) and SN 2013ak (Margutti et al. 2013) the source is the SN itself. A notable example is the case of SN 2008D, where the observation was taken only 10 d after the explosion, which is well recorded as it was serendipitously discovered by Soderberg et al. (2008) while observing a different SN in the same galaxy using the *Swift* X-ray telescope. The sources at the positions of SN 2004dk, SN 2009bb and 2014C (see Fig. 3 are most likely the SNe themselves as well given the timing of the observations, though we could not confirm these from literature. Note that SN 2009bb is partially blended with a nearby source. Because characterizing the properties of these sources is outside the scope of this paper, we did not attempt to disentangle them. Similarly, in the case of SN 1998bw, the source aperture actually contains two

Downloaded from http://mnras.oxfordjournals.org/ at University of Turku on February 1, 2016

Table 7. X-ray luminosities and upper limits of X-ray luminosity (post-explosion, part 2).

Name	(4) Accr. pulsar (high abs.)		(5) Hard-state BH (low abs.)		(6) Hard-state BH (high abs.)	
	Exp. map av. value ($cm^2 s$)	Luminosity ($erg\ s^{-1}$)	Exp. map av. value ($cm^2 s$)	Luminosity ($erg\ s^{-1}$)	Exp. map av. value ($cm^2 s$)	Luminosity ($erg\ s^{-1}$)
1983I	5.84×10^7	$<4.7 \times 10^{37}$	5.38×10^7	$<2.9 \times 10^{37}$	5.79×10^7	$<5.4 \times 10^{37}$
1983N	2.46×10^8	$<4.1 \times 10^{36}$	3.14×10^8	$<1.8 \times 10^{36}$	2.78×10^8	$<4.1 \times 10^{36}$
1983V	5.66×10^7	$<1.2 \times 10^{38}$	6.13×10^7	$<6.4 \times 10^{37}$	5.97×10^7	$<1.3 \times 10^{38}$
1984L	1.73×10^6	$<1.4 \times 10^{39}$	2.20×10^6	$<6.3 \times 10^{38}$	1.94×10^6	$<1.4 \times 10^{39}$
1985F	3.19×10^6	$<1.5 \times 10^{38}$	4.08×10^6	$<6.8 \times 10^{37}$	3.59×10^6	$<1.5 \times 10^{38}$
1990U	1.15×10^7	$<9.1 \times 10^{38}$	1.46×10^7	$<4.1 \times 10^{38}$	1.30×10^7	$<9.3 \times 10^{38}$
1991N	1.62×10^7	$(7.6\pm2.2) \times 10^{38}$	2.11×10^7	$(3.3\pm1.0) \times 10^{38}$	1.83×10^7	$(7.8\pm2.2) \times 10^{38}$
1993J	1.36×10^8	$(83.0\pm0.9) \times 10^{37}$	1.49×10^8	$(43.2\pm0.5) \times 10^{37}$	1.44×10^8	$(90.3\pm0.9) \times 10^{37}$
1994I	2.79×10^8	$(3.2\pm0.4) \times 10^{37}$	3.52×10^8	$(1.4\pm0.2) \times 10^{37}$	3.15×10^8	$(3.3\pm0.4) \times 10^{37}$
1996D	5.25×10^6	$<1.2 \times 10^{40}$	6.51×10^6	$<5.5 \times 10^{39}$	5.89×10^6	$<1.2 \times 10^{40}$
1996N	1.48×10^7	$<1.0 \times 10^{38}$	1.60×10^7	$<5.4 \times 10^{37}$	1.57×10^7	$<1.1 \times 10^{38}$
1996aq	2.38×10^6	$<1.6 \times 10^{39}$	3.01×10^6	$<7.1 \times 10^{38}$	2.67×10^6	$<1.6 \times 10^{39}$
1997X	3.28×10^6	$<1.3 \times 10^{38}$	4.28×10^6	$<5.8 \times 10^{37}$	3.70×10^6	$<1.3 \times 10^{38}$
1998T	4.01×10^7	$(2.0\pm0.1) \times 10^{40}$	4.93×10^7	$(9.4\pm0.6) \times 10^{39}$	4.47×10^7	$(2.1\pm0.1) \times 10^{40}$
1998bo	5.08×10^6	$<1.4 \times 10^{40}$	5.87×10^6	$<6.7 \times 10^{39}$	5.53×10^6	$<1.4 \times 10^{40}$
1998bw	1.66×10^7	$(4.9\pm0.6) \times 10^{39}$	2.18×10^7	$(2.1\pm0.2) \times 10^{39}$	1.87×10^7	$(5.0\pm0.6) \times 10^{39}$
1999dn	1.92×10^7	$<9.8 \times 10^{38}$	2.48×10^7	$<4.3 \times 10^{38}$	2.16×10^7	$<1.0 \times 10^{39}$
1999eh	5.90×10^6	$<1.1 \times 10^{39}$	7.57×10^6	$<4.9 \times 10^{38}$	6.67×10^6	$<1.1 \times 10^{39}$
1999ex	3.89×10^6	$<5.8 \times 10^{39}$	4.95×10^6	$<2.6 \times 10^{39}$	4.38×10^6	$<6.0 \times 10^{39}$
2000cr	5.33×10^6	$<2.3 \times 10^{39}$	6.79×10^6	$<1.0 \times 10^{39}$	6.00×10^6	$<2.4 \times 10^{39}$
2000ds	2.17×10^7	$<3.7 \times 10^{38}$	2.78×10^7	$<1.7 \times 10^{38}$	2.44×10^7	$<3.8 \times 10^{38}$
2001ig	1.63×10^7	$(2.4\pm0.4) \times 10^{38}$	2.14×10^7	$(1.0\pm0.2) \times 10^{38}$	1.85×10^7	$(2.4\pm0.4) \times 10^{38}$
2003L	1.03×10^7	$(2.7\pm0.5) \times 10^{40}$	1.35×10^7	$(1.2\pm0.2) \times 10^{40}$	1.17×10^7	$(2.8\pm0.5) \times 10^{40}$
2003bg	4.30×10^7	$(3.5\pm0.1) \times 10^{39}$	5.57×10^7	$(15.4\pm0.6) \times 10^{38}$	4.85×10^7	$(3.6\pm0.1) \times 10^{39}$
2003is	2.52×10^6	$<1.4 \times 10^{40}$	2.82×10^6	$<7.0 \times 10^{39}$	2.78×10^6	$<1.4 \times 10^{40}$
2004C	4.66×10^7	$(1.6\pm0.2) \times 10^{39}$	5.99×10^7	$(7.0\pm0.8) \times 10^{38}$	5.25×10^7	$(1.6\pm0.2) \times 10^{39}$
2004dk	2.75×10^6	$(1.2^{+0.7}_{-0.5}) \times 10^{39}$	3.48×10^6	$(5.3^{+3.1}_{-2.1}) \times 10^{38}$	3.09×10^6	$(1.2^{+0.7}_{-0.5}) \times 10^{39}$
2005U	3.38×10^7	$(2.3\pm0.6) \times 10^{39}$	4.19×10^7	$(1.1\pm0.3) \times 10^{39}$	3.79×10^7	$(2.3\pm0.6) \times 10^{39}$
2005at	1.59×10^7	$<3.7 \times 10^{37}$	1.71×10^7	$<2.0 \times 10^{37}$	1.69×10^7	$<4.0 \times 10^{37}$
2005cz	4.70×10^6	$<1.0 \times 10^{39}$	6.02×10^6	$<4.6 \times 10^{38}$	5.29×10^6	$<1.0 \times 10^{39}$
2006ep	2.73×10^6	$<9.2 \times 10^{39}$	3.48×10^6	$<4.1 \times 10^{39}$	3.08×10^6	$<9.4 \times 10^{39}$
2007Y	1.48×10^7	$<2.3 \times 10^{38}$	1.61×10^7	$<1.2 \times 10^{38}$	1.58×10^7	$<2.5 \times 10^{38}$
2007gr	5.99×10^6	$<1.6 \times 10^{38}$	6.73×10^6	$<8.1 \times 10^{37}$	6.41×10^6	$<1.7 \times 10^{38}$
2007ke	3.98×10^7	$<1.4 \times 10^{40}$	4.46×10^7	$<7.1 \times 10^{39}$	4.26×10^7	$<1.5 \times 10^{40}$
2008D	6.03×10^6	$(1.3^{+0.6}_{-0.4}) \times 10^{39}$	7.70×10^6	$(6.0^{+2.6}_{-1.9}) \times 10^{38}$	6.80×10^6	$(1.4^{+0.6}_{-0.4}) \times 10^{39}$
2008bo	6.57×10^6	$<7.2 \times 10^{38}$	8.35×10^6	$<3.2 \times 10^{38}$	7.39×10^6	$<7.4 \times 10^{38}$
2009bb	3.40×10^6	$(3.5^{+1.8}_{-1.3}) \times 10^{39}$	4.32×10^6	$(1.6^{+0.8}_{-0.6}) \times 10^{39}$	3.82×10^6	$(3.6^{+1.9}_{-1.4}) \times 10^{39}$
2009jf	3.44×10^6	$(2.4\pm0.3) \times 10^{40}$	4.36×10^6	$(1.1\pm0.1) \times 10^{40}$	3.86×10^6	$(2.4\pm0.3) \times 10^{40}$
2009mk	3.39×10^6	$<9.6 \times 10^{38}$	4.29×10^6	$<4.3 \times 10^{38}$	3.82×10^6	$<9.8 \times 10^{38}$
2010O	3.03×10^7	$(3.6\pm0.2) \times 10^{40}$	3.75×10^7	$(16.5\pm0.9) \times 10^{39}$	3.40×10^7	$(3.7\pm0.2) \times 10^{40}$
2011dh	2.55×10^8	$(24.8\pm0.7) \times 10^{37}$	3.17×10^8	$(11.4\pm0.3) \times 10^{37}$	2.86×10^8	$(25.3\pm0.8) \times 10^{37}$
2011ei	3.34×10^6	$<3.0 \times 10^{39}$	4.18×10^6	$<1.4 \times 10^{39}$	3.75×10^6	$<3.1 \times 10^{39}$
2012ap	3.33×10^6	$<7.4 \times 10^{39}$	4.16×10^6	$<3.4 \times 10^{39}$	3.74×10^6	$<7.5 \times 10^{39}$
2013ak	3.33×10^6	$(1.1\pm0.2) \times 10^{39}$	4.11×10^6	$(5.0\pm0.9) \times 10^{38}$	3.73×10^6	$(1.1\pm0.2) \times 10^{39}$
2013ge	6.25×10^6	$<3.5 \times 10^{38}$	7.68×10^6	$<1.6 \times 10^{38}$	7.00×10^6	$<3.5 \times 10^{38}$
2014C	6.58×10^6	$(16.0\pm0.7) \times 10^{39}$	7.86×10^6	$(7.6\pm0.3) \times 10^{39}$	7.34×10^6	$(16.5\pm0.7) \times 10^{39}$

Note that the luminosities presented here do not accurately reflect the luminosity of SNe due to chosen spectral models or multi-epoch stacking of observations.

sources at close proximity (Fig. 4), of which the source closer to the centre of the source aperture is SN 1998bw (for details, see Kouveliotou et al. 2004). Again, because the sources partially overlap, we did not attempt to disentangle them.

SN 1998T and SN 2005U are in the same galaxy as SN 2010O, Arp 299, and in close enough proximity to each other (∼2.5 arcsec) that their source apertures partially overlap. Similar to SN 2010O, the region is very complex and it is difficult to identify particularly faint sources from the area. The position of SN 1998T overlaps with a known ULX, [ZWM2003] 12 (Zezas, Ward & Murray 2003), which we identify as the source. SN 2005U had both pre- and post-explosion data available, and for both measurements we excluded the ULX and other interfering sources (see Fig. 4) from both the background and the source aperture. Although this produces an apparent detection at the position of SN 2005U post-explosion (the flux from within the defined source aperture exceeds the background by 3σ), we associate this with the inhomogeneous distribution of diffuse emission in the region, rather than any point-sources within the aperture (the reason why this signal is not apparent in the pre-explosion observation is likely due to the shorter exposure time – the luminosity of this apparent source is lower than the upper limit established for the pre-explosion case). The measured luminosities presented in Tables 6 and 7 for this SN should therefore be mainly treated as upper limits.

Downloaded from http://mnras.oxfordjournals.org/ at University of Turku on February 1, 2016

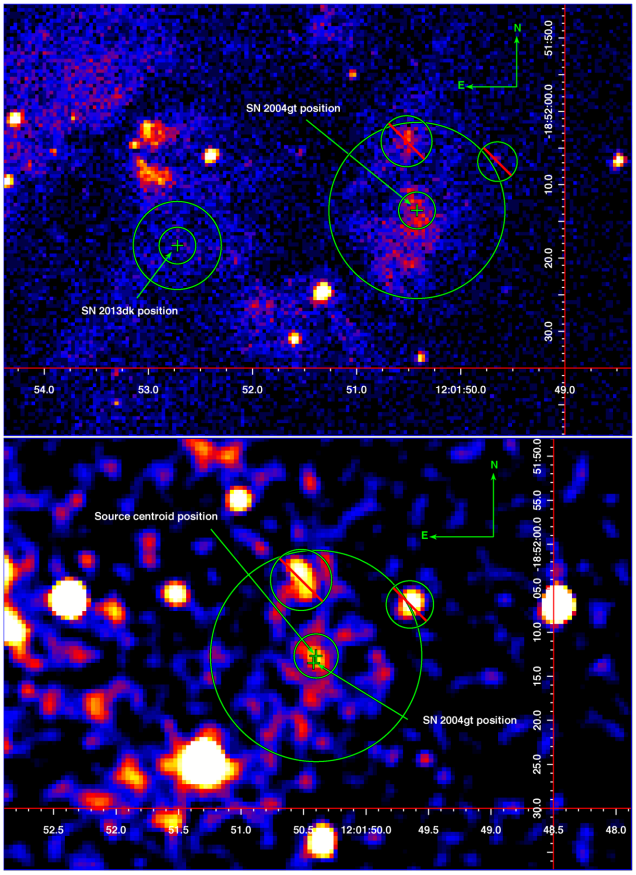

Figure 1. Top: SN 2013dk and SN 2004gt (pre-explosion), at the 0.5–7.0 keV energy range. The inner circles are the source apertures, surrounded by the background annuli. The radius of the source aperture is 2.5 arcsec for both cases, and the outer radii of the background annuli are 6 and 12 arcsec, respectively. The apertures are centred on the SN positions. Bottom: the source (CXOU J120150.4−185212) and our measured position of SN 2004gt (pre-explosion) at 1.5–8.0 keV energy range. The central circle is the source aperture (radius 2.5 arcsec) centred on the centroid of the source, and the annulus (outer radius 12 arcsec) around it is the background extraction area. The circles with red bars contain unrelated sources which were excluded from the background extraction area. Each image pixel corresponds to ∼0.5 arcsec. FWHM=3-pixel Gaussian smoothing has been applied to the bottom image to make the source more visible.

In the case of SN 1994I we see three faint point sources inside the source aperture, one of which appears to be very close to the SN position, but overall all three are relatively faint and within *Chandra's* 90 per cent encircled energy radius for the PSF which makes associating any of them with a particular source within this source aperture unreliable, although the central one most likely is the SN (also see Immler, Wilson & Terashima 2002). For the purposes of this study and unlike in the case of SN 1998bw, because the sources do not overlap as clearly, we have excluded the other sources and measured the central source, assuming it to be the SN. Similarly, with SN 1991N, the source region is extremely crowded, with high background emission and multiple nearby bright point sources. There are also several possible sources inside the source aperture which cannot be directly associated with the SN position or identified with confidence to exclude, which together produce enough flux to rate as a false detection.

Finally, in the case of SN 1983I, we note that there is some uncertainty to the coordinates of this SN (Asiago catalogue only reports the coordinates of the host galaxy, while USC and SSC both report different coordinates ∼2 arcsec apart[10]). The coordinates used in this study are those reported by USC. There is a clear X-ray point-source ∼3 arcsec from the USC position which we were unable to conclusively identify and therefore cannot rule out that this is actually SN 1983I. Note that the luminosities for post-explosion sources presented in this paper are not directly representative of the SNe, as our models represent HMXBs and were not fitted to the individual spectra of the SNe. Similarly, some of the measurements (such as those of SN 1993J) involved stacking observations across multiple epochs over a potentially long time-period, and therefore would include any variability in the source during that time frame.

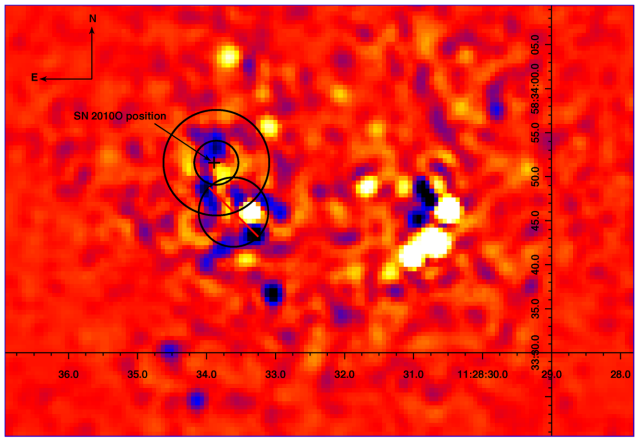

Figure 2. Exposure-corrected difference-map of SN 2010O position in Arp 299 ($cm^{-2}s^{-1}$) (Spectral model: 1 keV blackbody, $N_H = 0.5 \times 10^{22}$ cm^{-2}, darker areas indicate reduction in flux in the post-explosion data). FWHM=3-pixel Gaussian smoothing has been applied to the image. The concentric circles depict the source aperture and the background region used for extraction. The circle with a red bar contains numerous unrelated bright sources which were excluded from the extraction area. The cross marks the position of the transient source found by Nelemans et al. (2010).

4.3 SN luminosity upper limits

Figs 5 and 6 show the measured upper limits plotted for the six spectral models used. Targets with a detection above 3σ are not included. Because WR-stars as a part of HMXB systems will result in stripped-envelope SNe, in both plots we also compare our results against the luminosities of the three WR X-ray binaries that are known to exist. These are NGC 300 X-1 with average unabsorbed luminosity 4.1×10^{38} erg s^{-1} (Carpano et al. 2007), IC 10 X-1 with unabsorbed luminosity 1.8×10^{38} erg s^{-1} (Bauer & Brandt 2004) and Cygnus X-3, presented in two modes: quiescent with $L = 1.4 \times 10^{37}$ erg s^{-1} and hypersoft with $L = 5.7 \times 10^{37}$ erg s^{-1} (both from McCollough, Smith & Valencic 2013, representing the states with the lowest and highest X-ray fluxes, respectively). A fourth candidate WR-binary CXOU J004732.0−251722.1 in the galaxy NGC 253 identified by Maccarone et al. (2014) is also included (with unabsorbed luminosity $L = 9.9 \times 10^{37}$ erg s^{-1}). The aforementioned luminosities have been re-scaled to our 0.5–7.0 keV energy range from their original values. Finally, we also include a comparison to ULX, which are defined as sources with X-ray luminosity above 1×10^{39} erg s^{-1}.

[10] Both calculated from the same nuclear offsets, possibly based on Tsvetkov (1985), which may have a high uncertainty.

Downloaded from http://mnras.oxfordjournals.org/ at University of Turku on February 1, 2016

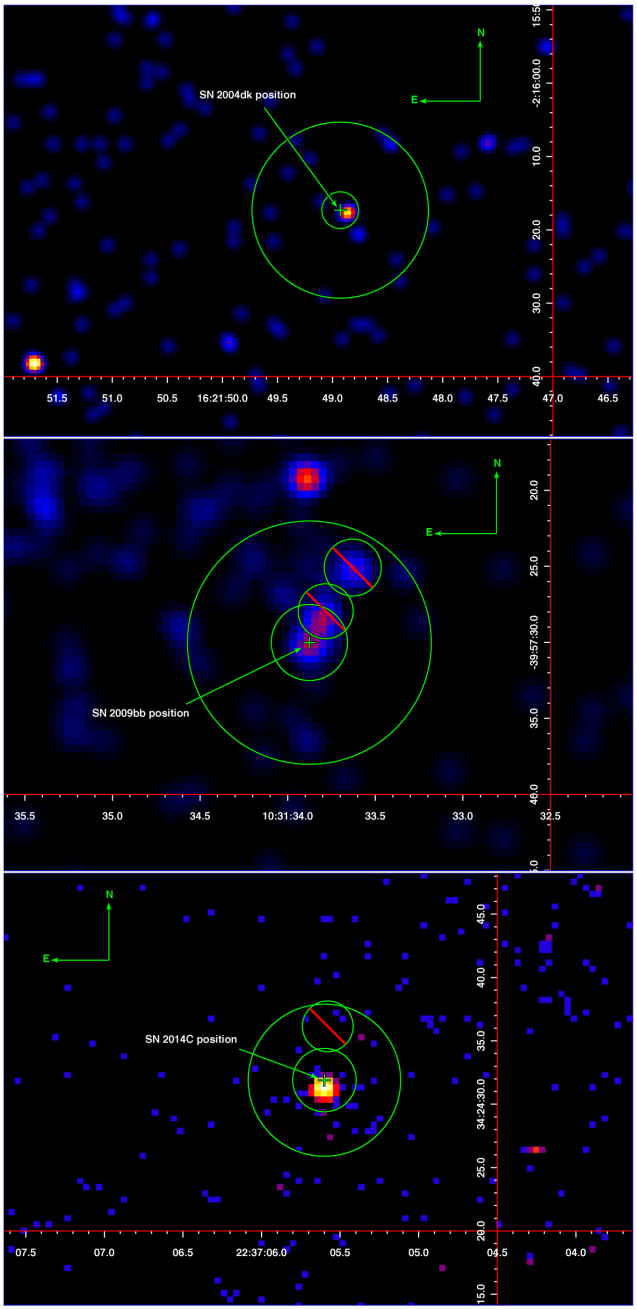

Figure 3. The post-explosion sources at the positions of SN 2004dk, SN 2009bb and SN 2014C. FWHM=3-pixel Gaussian smoothing has been applied to the images of SN 2004 dk and SN 2009bb to make the sources more visible. The circles with red bars contains sources which were excluded from the extraction areas. The exclusion-circle near SN 2014C is at the position of a variable source visible in the pre-explosion data. Note that the source at SN 2009bb position partially blends with a nearby excluded source.

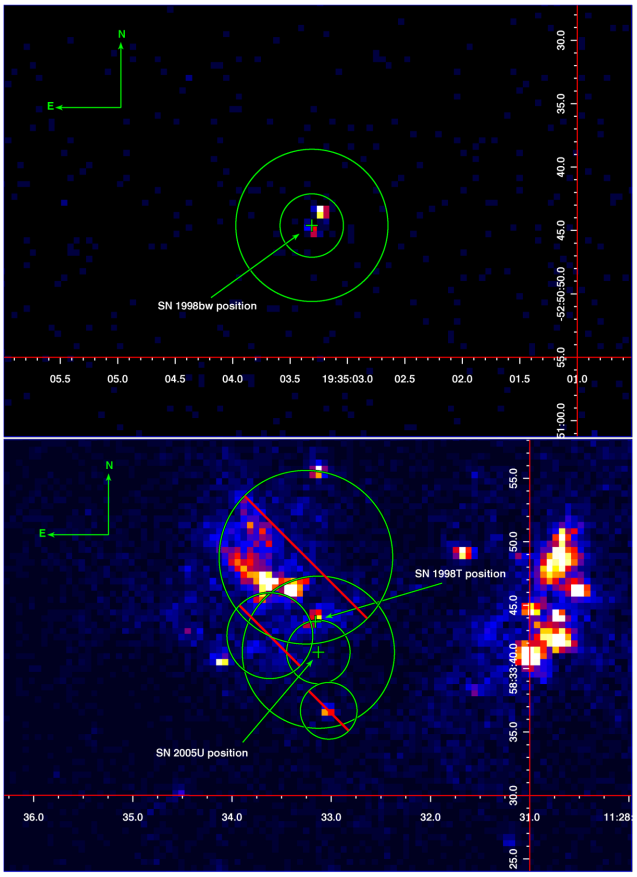

Figure 4. Top: SN 1998bw position (post-explosion). Bottom: SN 2005U position (post-explosion). The central circle is the source extraction area and the annulus around it is the background extraction area. The circles with red bars contain unrelated sources which were excluded from the extraction area. The relative location of SN 1998T is also marked.

4.4 Fraction of X-ray bright progenitor systems

There are two requirements for a progenitor to be a luminous X-ray source in a pre-explosion observation. The first is for the progenitor star to have a compact object as a binary companion. The second is that the binary separation must be small enough for the progenitor to supply mass to the companion, either by Roche lobe overflow or stellar wind, to produce the X-ray luminosity.

We have attempted to gain an estimate of the number of binary systems that might be luminous in X-rays when the system explodes. We have used the latest version (2.0) of the Binary Population and Spectral Synthesis, BPASS, stellar population models (Eldridge, Izzard & Tout 2008; Eldridge & Stanway 2009; Eldridge et al. in preparation: http://bpass.auckland.ac.nz). The stellar population included stars at solar metallicity with initial masses from 0.1 to 300 $M_{\odot}$. We determined the mass of the primary using a Salpeter initial mass function with a slope of -2.35. We then use a binary period distribution that is flat in log of the period and flat in mass ratio distribution to determine the mass of the secondary. These are consistent with the distributions observed by Sana et al. (2012). The orbits are assumed to be circular. While observed binaries have eccentric orbits, we note that if the stars are close enough to interact, circularization will most likely have occurred and, as found by Hurley, Tout & Pols (2002), a full treatment of eccentricity is not generally required in population synthesis.

We assume that a star explodes if it has a final mass greater than 2 $M_{\odot}$ and a CO core mass greater than 1.38 $M_{\odot}$. We count the stellar models which will explode as Type Ib, Ic or IIb SNe being those which have less than 0.5 $M_{\odot}$ hydrogen at the point of core-collapse. We then also record each event that occurs within a

Downloaded from http://mnras.oxfordjournals.org/ at University of Turku on February 1, 2016

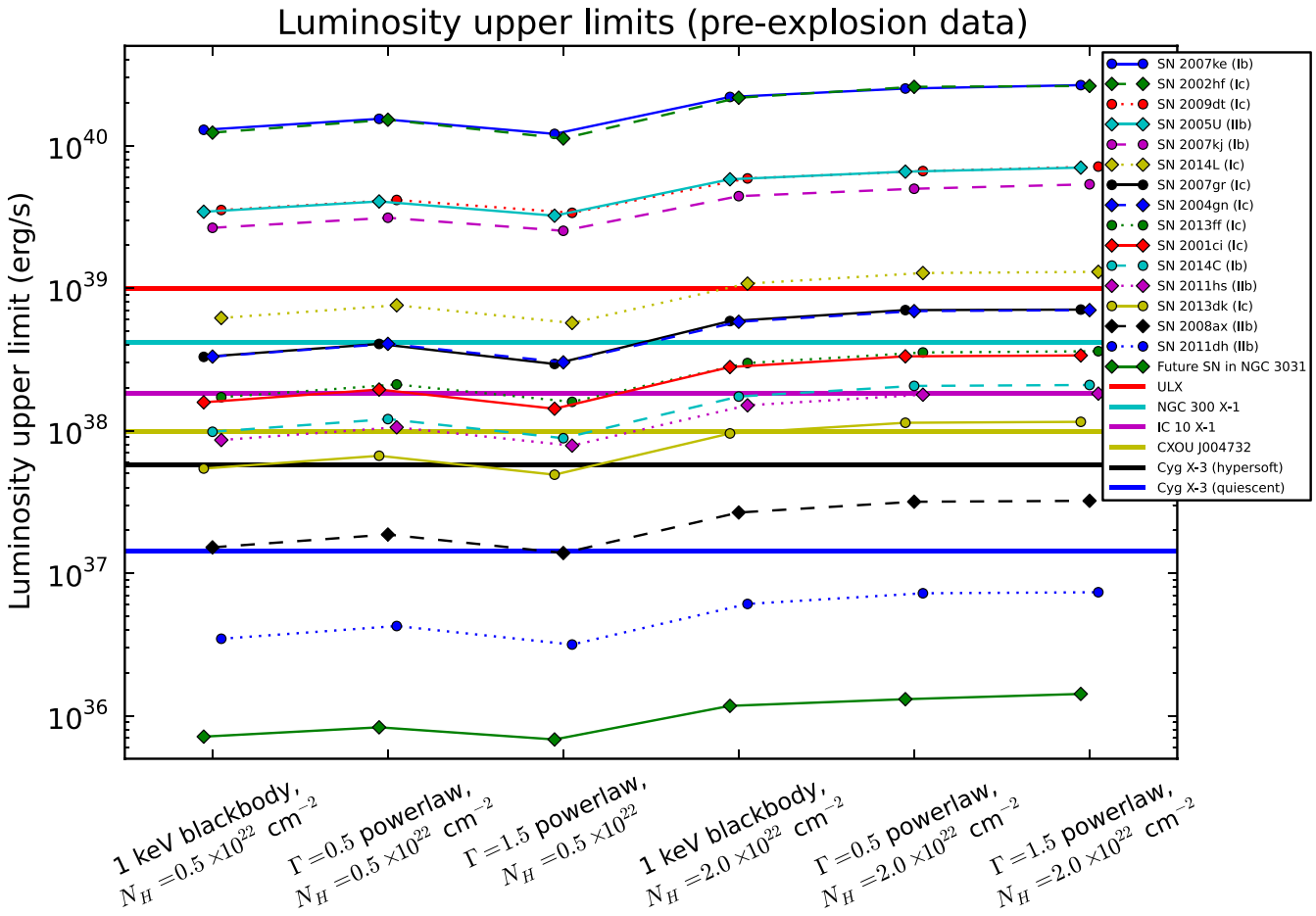

Figure 5. Pre-explosion luminosity upper limits. SNe with a detected source are not included (for details, see Section 4.1).

binary with a compact object where the size of the progenitor model is comparable to the size of the orbit and therefore is likely to be emitting X-rays via either Roche lobe overflow or by wind accretion. This is a simple way to estimate the number of progenitors that might be in X-ray binary systems. We also separately record SNe that are the first ones to occur in the binary system, although these are less likely to be detectable in pre-explosion X-ray observations, as wind–wind collision systems have much weaker X-ray emission than HMXBs.

We show these estimates in Table 8, where the first column is the lower limit for the ratio of the SN progenitor's radius to the binary separation. The second column shows the percentage of all stripped-envelope SNe (in binary systems) that have the corresponding or higher ratio of progenitor radius to binary separation. The third column is the same as the second one, except only for systems where the progenitor's companion has already exploded as an SN, producing a compact object. From this, we can see that the fraction of stripped envelope progenitor systems that are likely to be luminous X-ray sources is only up to a few per cent. This number could be significantly higher if close binaries without a compact object, where stellar winds interact and produce X-rays (with significantly lower luminosities), were also included. However, the values provided by our modelling are uncertain and depend on many factors. They could be increased if, for example, mass-transfer is more efficient than assumed or SN kicks are weaker than assumed. We therefore stress that these values are only rough estimates, but they do at least indicate the order of magnitude for the expected rate.

4.5 Upper limits for future nearby SNe

In order to investigate the potential of the presented method for constraining the progenitor system of a future SN in a nearby galaxy, we measured the upper limit of unabsorbed luminosity for an empty field in the host galaxy of SN 1993J, NGC 3031, 10.2 arcsec north-east of the SN and using the same set of observations. We chose this galaxy not only because it is the host to the closest SN in our sample (at distance 3.63 Mpc), but also because it has one of the longest combined exposure times available (752.3 ks). The extraction area was a circular aperture with 2.5 arcsec radius, which was found to contain 24 photons for the combined observation. For the spectral models used in this study, the range of upper limits of luminosity (corrected for absorption) obtained were $L_{\rm UL} = (0.7–1.4) \times 10^{36}$ erg s^{-1} for models 5 and 6, respectively, with other models falling between these values. This gives us a reasonable estimate for the faintest progenitor source that could be detected for a future extragalactic SN. It is notable that this is almost an order of magnitude fainter than the quiescent state of Cygnus X-3, the closest and faintest known WR X-ray binary at the distance of ∼9 kpc (McCollough et al. 2013).

5 DISCUSSION

Of the 18 SNe with pre-explosion data available, three were found to have flux above the 3σ detection threshold at their positions. Two of these are identifiable point sources and possible candidates

Downloaded from http://mnras.oxfordjournals.org/ at University of Turku on February 1, 2016

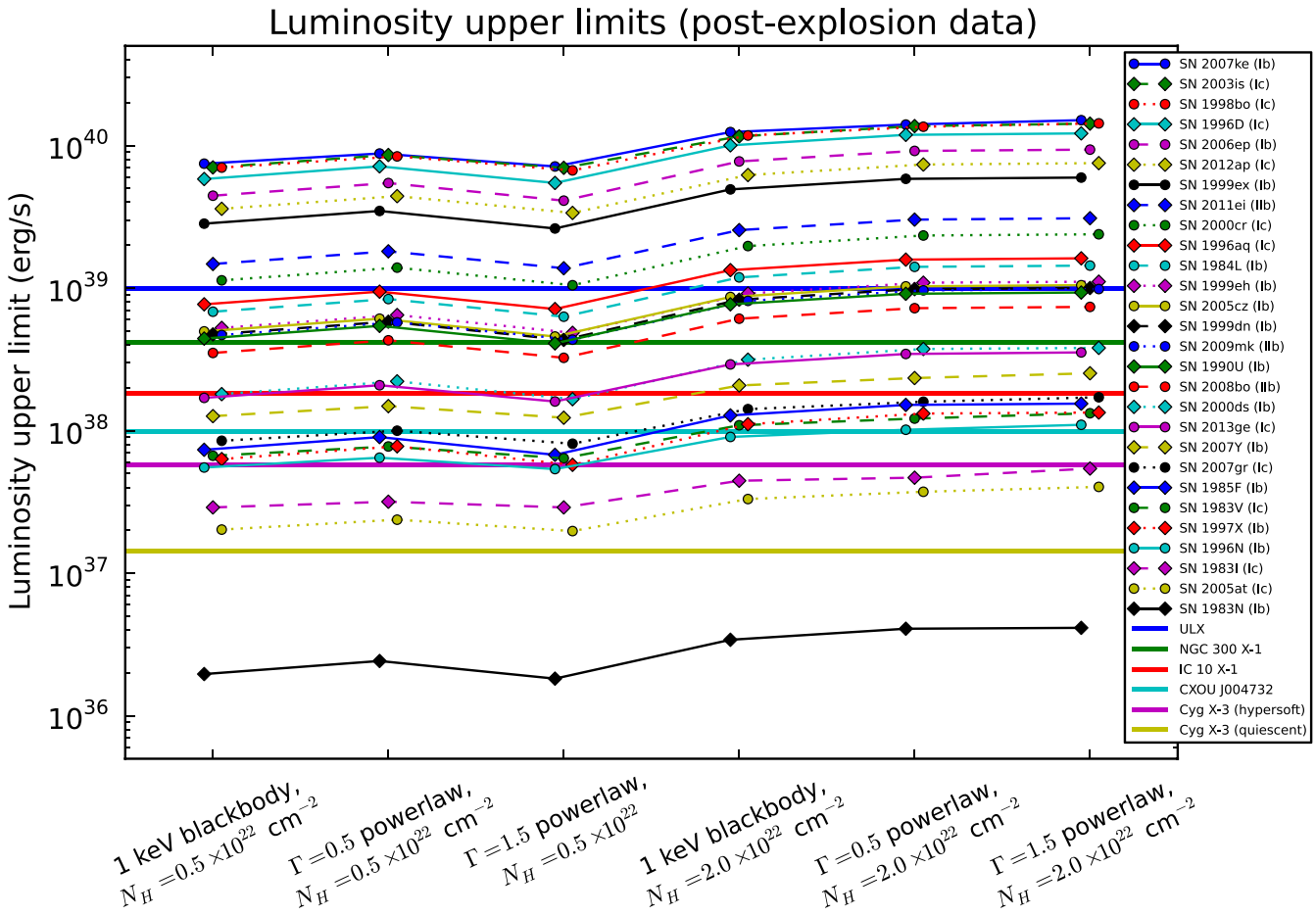

Figure 6. Post-explosion luminosity upper limits. SNe with detected source are not included (for details, see Section 4.1).

Table 8. Stripped envelope SN progenitors as a function of binary separation.

Ratio of progenitor radius to separation, (R_*/a)	Fraction of binary systems with a normal companion	Fraction of binary systems with a compact companion
>1	0.07	0.004
>0.5	0.18	0.009
>0.1	0.39	0.018
>0.01	0.72	0.026

for an HMXB SN progenitor, both previously known sources. The possible association between the ULX CXOU J230453.0+121959 and SN 2009jf was already suggested by Voss et al. (2011). We also consider it possible that CXOU J120150.4−185212 might be associated with the progenitor of SN 2004gt. Mineo, Gilfanov & Sunyaev (2012) categorized this source as an HMXB based on its relative position within the host galaxy, and although we note that this categorization is purely statistical and has not been confirmed observationally, it does suggest that the source can plausibly be considered an HMXB progenitor candidate for the SN. The lack of post-explosion data for SN 2004gt prevents the determination of any variability in this source, however. Given that over a decade has passed since the explosion of SN 2004gt, the SN may have faded enough that it might be possible in the near future to measure this source again for possible variability, although given the relative faintness of the source in the pre-explosion data (with luminosity $\sim 5 \times 10^{37}$ erg s^{-1}) and the overall complexity of the region, this may be difficult. The third detection is at the location of SN 2010O, which contains a complex system of multiple variable sources. There is a possibility that SN 2010O has an X-ray bright progenitor as suggested by Nelemans et al. (2010), although as noted previously, the complexity of the region makes associating any particular source with the SN difficult. All three of the aforementioned potential associations between X-ray sources and their corresponding SNe remain uncertain, however.

One SN in our sample, SN 2008ax is known to not have an HMXB progenitor from optical pre-explosion data. However, for the 14 other SNe, X-ray luminosity upper limits were established, constraining the properties of any progenitor systems. Although all possible HMXB progenitor systems cannot be ruled out based on these limits, some of the most luminous cases can be excluded. Specifically, a ULX progenitor could be ruled out for 9 out of 14 SNe in the sample. For one of these SNe, SN 2011dh, optical pre-explosion observations had previously identified a yellow supergiant progenitor in a binary system. However, the recent observations by Maund et al. (2015) suggest that the companion to the progenitor is either fainter than previously believed, or may not exist at all. As the nature of the companion, if one exists, is uncertain, SN 2011dh makes an interesting target for our study. The relatively low upper limit of X-ray luminosity evident from our results could be taken as an indication that this SN did not have an HMXB progenitor.

Downloaded from http://mnras.oxfordjournals.org/ at University of Turku on February 1, 2016

We also compared the upper limits to the luminosities of the three known (and one candidate) WR X-ray binaries, a type of HMXB likely to produce a stripped-envelope CCSN. The known WR HMXBs tend to be more X-ray luminous than HMXBs on average: NGC 300 X-1, IC 10 X-1 and CXOU J004732 all have X-ray luminosities that are higher than 10^{38} erg s^{-1}, whereas the majority of HMXBs appear to be less luminous (see e.g. Mineo et al. 2012). However, the case of Cygnus X-3, the only known WR X-ray binary in our own galaxy, demonstrates both that much fainter systems of this nature can exist and that their luminosity can be greatly variable depending on the state of the system. In general, given the relative rarity of WR-HMXBs, it is quite likely that there is an observational bias favouring the detection of only these brighter systems. The upper limits obtained in this study are mostly comparable to the average luminosity of the known WR-HMXBs, suggesting that such systems could in principle have been detected.

One problem inherent in interpreting pre-explosion X-ray observations is that it is not known whether or not accretion from the progenitor to the compact companion continues all the way to the explosion, and if not, how long before the core-collapse it would shut down. Because this accretion is the source of X-ray flux from the assumed progenitor system, it is possible that the system has ceased to be a luminous X-ray source before the SN on a time-scale which would make pre-explosion detection impractical or impossible. Our BPASS-modelling discussed earlier indicates that, while a significant number of stripped-envelope SN progenitors can be expected to be found in binary systems, only a small fraction of these would contain a compact companion at a binary separation where substantial mass-transfer could be expected to occur. HMXB-type progenitors would therefore be quite rare. The possibility of observing X-rays from non-HMXB progenitors remains, but such objects would most likely be relatively faint (comparable to a WR-star), and well below the threshold found in this study.

One way to constrain the time frame in which a progenitor system might become X-ray bright is to observe HMXBs that are associated with supernova remnants (SNRs). SNRs are relatively short-lived, so this would help establish how soon after the SN accretion might be initiated in a newly formed HMXB. Several such systems have been identified, for example SXP 1062 (Hénault-Brunet et al. 2012) and DEM L241 (Seward et al. 2012), both of which have an estimated age of several times 10^4 yr. Another possible case is Circinus X-1, for which Heinz et al. (2013) derive an age upper limit of $\sim$4600 yr. While none of these systems are X-ray luminous enough to allow detection by our study, these examples indicate that accretion in a newly formed HMXB might begin on a time-scale that is less than a few thousand years after the SN. Another example to consider is the association between SNR W50 and SS 433, although it is estimated to be older than the aforementioned cases (see e.g. Goodall, Alouani-Bibi & Blundell 2011).

X-ray binaries are not the only type of pre-explosion X-ray source that might be associated with an SN. Colliding wind binaries, such as the luminous blue variable binary Eta Carinae, or the WR binary WR 48a, are known to have X-ray luminosities up to $\sim 10^{35}$ erg s^{-1} (see e.g. Zhekov, Gagné & Skinner 2011; Nazé, Rauw & Hutsemékers 2012; Hamaguchi et al. 2014a). Compared to the upper limits we derived, such objects are an order of magnitude fainter than what could reasonably be detected with *Chandra*, unless they were significantly closer. Also, given that e.g. Eta Carinae is known to have a fairly hard X-ray spectrum (e.g. Hamaguchi et al. 2014b), they would likely be difficult to distinguish from HMXBs based on their spectrum alone. Future studies are therefore unlikely to find such SN progenitors using this method.

6 CONCLUSIONS

The aim of this study was to examine the possibility of HMXBs being the progenitors to some stripped-envelope CCSNe with a direct observational test, or to constrain the possibility of such progenitors in the sample. If an SN progenitor was part of an HMXB before the explosion, the system could be an X-ray source due to accretion from the progenitor star to the compact object. In this study, we note the existence of two pre-explosion sources that could potentially be associated with SNe. The first of these is the ULX CXOU J230453.0+121959 at the position of the Type Ib SN 2009jf (Voss et al. 2011), with luminosity $\sim 1 \times 10^{40}$ erg s^{-1}. The second candidate is CXOU J120150.4−185212, at the position of the Type Ic SN 2004gt, with luminosity $\sim 5 \times 10^{37}$ erg s^{-1}. For both of these, however, it is important to note that chance co-alignment is possible. We also measure the unabsorbed pre-explosion upper limits of X-ray luminosity for the positions of 14 stripped-envelope CCSNe. Most of the upper limits obtained are comparable to the luminosities of the two known and one candidate extragalactic WR-HMXBs, showing that at least more luminous examples of such systems could in principle have been detected. Therefore, while detecting a candidate progenitor in this way is possible, the existence of one cannot be completely ruled out without using significantly deeper exposure times or observing much more nearby SNe. The main limiting factor to future studies using this method is the scarcity of deep pre-explosion observations. We found that such *Chandra* data exists only for $\sim$6 per cent of SNe within $\sim$100 Mpc distance. Furthermore, our modelling indicates that HMXB-progenitor systems would likely be quite rare. However, these numbers could be increased if mass-transfer between the binary components is more efficient or SN kicks are weaker than assumed. The long X-ray luminosity decline time of most SNe of these types (see e.g. Dwarkadas & Gruszko 2012) limits the usefulness of post-explosion observations for recent SNe but could potentially allow the confirmation of candidate HMXB progenitors, once the SN has faded sufficiently.

ACKNOWLEDGEMENTS

We thank the referee for their helpful comments and feedback. This research has made use of data obtained from the Chandra Data Archive and the Chandra Source Catalog, and software provided by the Chandra X-ray Center (CXC) in the application packages CIAO, CHIPS, and SHERPA. This research has made use of the NASA/IPAC Extragalactic Database (NED) which is operated by the Jet Propulsion Laboratory, California Institute of Technology, under contract with the National Aeronautics and Space Administration. This publication makes use of data products from the Two Micron All Sky Survey, which is a joint project of the University of Massachusetts and the Infrared Processing and Analysis Center/California Institute of Technology, funded by the National Aeronautics and Space Administration and the National Science Foundation. This research has made use of the VizieR catalogue access tool, CDS, Strasbourg, France (Ochsenbein, Bauer & Marcout 2000). We also acknowledge the use of the Hyperleda data base (http://leda.univ-lyon1.fr). The plots in this paper were made using MATPLOTLIB (Hunter 2007), http://matplotlib.org. This research has made use of NASA's Astrophysics Data System. This research was partly supported by the European Union FP7 programme through ERC grant number 320360.

Downloaded from http://mnras.oxfordjournals.org/ at University of Turku on February 1, 2016

REFERENCES

Alard C., 2000, A&AS, 144, 363
Alard C., Lupton R. H., 1998, ApJ, 503, 325
Aldering G., Humphreys R. M., Richmond M., 1994, AJ, 107, 662
Barbon R., Buondí V., Cappellaro E., Turatto M., 1999, A&AS, 139, 531
Bauer F. E., Brandt W. N., 2004, ApJ, 601, L67
Bersten M. C. et al., 2014, AJ, 148, 68
Bietenholz M. F. et al., 2010, ApJ, 725, 4
Bufano F. et al., 2014, MNRAS, 439, 1807
Cao Y. et al., 2013, ApJ, 775, L7
Carpano S., Pollock A. M. T., Wilms J., Ehle M., Schirmer M., 2007, A&A, 461, L9
Chandra P., Dwarkadas V. V., Ray A., Immler S., Pooley D., 2009, ApJ, 699, 388
Crockett R. M. et al., 2008, MNRAS, 391, L5
Crowther P. A., 2007, ARA&A, 45, 177
Dominici T. P., Teixeira R., Horvath J. E., Holvorcem P., 1998, IAU Circ., 6946, 3
Dwarkadas V. V., Gruszko J., 2012, MNRAS, 419, 1515
Eldridge J. J., Stanway E. R., 2009, MNRAS, 400, 1019
Eldridge J. J., Izzard R. G., Tout C. A., 2008, MNRAS, 384, 1109
Eldridge J. J., Fraser M., Smartt S. J., Maund J. R., Crockett R. M., 2013, MNRAS, 436, 774
Eldridge J. J., Fraser M., Maund J. R., Smartt S. J., 2015, MNRAS, 446, 2689
Ergon M. et al., 2014, A&A, 562, A17
Filippenko A. V., 1997, ARA&A, 35, 309
Filippenko A. V., Chornock R., 2001, IAU Circ., 7638, 1
Fiorentino G., Musella I., Marconi M., 2013, MNRAS, 434, 2866
Folatelli G. et al., 2014, ApJ, 793, L22
Fremling C. et al., 2014, A&A, 565, A114
Gal-Yam A., Mazzali P. A., Manulis I., Bishop D., 2013, PASP, 125, 749
Ganeshalingam M., Li W., Filippenko A. V., 2013, MNRAS, 433, 2240
Gehrels N., 1986, ApJ, 303, 336
Gerke J. R., Kochanek C. S., Prieto J. L., Stanek K. Z., Macri L. M., 2011, ApJ, 743, 176
Gerke J. R., Kochanek C. S., Stanek K. Z., 2015, MNRAS, 450, 3289
Goodall P. T., Alouani-Bibi F., Blundell K. M., 2011, MNRAS, 414, 2838
Hamaguchi K. et al., 2014a, ApJ, 784, 125
Hamaguchi K. et al., 2014b, ApJ, 795, 119
Heinz S. et al., 2013, ApJ, 779, 171
Hénault-Brunet V. et al., 2012, MNRAS, 420, L13
Hicken M., Wood-Vasey W. M., Blondin S., Challis P., Jha S., Kelly P. L., Rest A., Kirshner R. P., 2009, ApJ, 700, 1097
Hunter J. D., 2007, Comput. Sci. Eng., 9, 90
Hunter D. J. et al., 2009, A&A, 508, 371
Hurley J. R., Tout C. A., Pols O. R., 2002, MNRAS, 329, 897
Immler S., Wilson A. S., Terashima Y., 2002, ApJ, 573, L27
Jha S., Riess A. G., Kirshner R. P., 2007, ApJ, 659, 122
Kangas T., Mattila S., Kankare E., Kotilainen J. K., Väisänen P., Greimel R., Takalo A., 2013, MNRAS, 436, 3464
Karachentsev I. D., Makarov D. I., Kaisina E. I., 2013, AJ, 145, 101
Kouveliotou C. et al., 2004, ApJ, 608, 872
Kuncarayakti H. et al., 2015, A&A, 579, A95
Lennarz D., Altmann D., Wiebusch C., 2012, A&A, 538, A120
Lyman J., Bersier D., James P., Mazzali P., Eldridge J., Fraser M., Pian E., 2014, preprint (arXiv:1406.3667)
Maccarone T. J., Lehmer B. D., Leyder J. C., Antoniou V., Hornschemeier A., Ptak A., Wik D., Zezas A., 2014, MNRAS, 439, 3064
McCollough M. L., Smith R. K., Valencic L. A., 2013, ApJ, 762, 2
Maeda K., Katsuda S., Bamba A., Terada Y., Fukazawa Y., 2014, ApJ, 785, 95
Mandel K. S., Wood-Vasey W. M., Friedman A. S., Kirshner R. P., 2009, ApJ, 704, 629
Mandel K. S., Narayan G., Kirshner R. P., 2011, ApJ, 731, 120
Marcaide J. M. et al., 1993, IAU Circ., 5820, 2
Margutti R., Soderberg A., Chakraborti S., Drout M., Kamble A., Milisavljevic D., Sanders N., Zauderer A., 2013, Astron. Telegram, 4944, 1
Mattila S., Meikle W. P. S., Greimel R., 2004, New Astron. Rev., 48, 595
Mattila S., Monard L. A. G., Li W., 2005, IAU Circ., 8473, 2
Mattila S. et al., 2012, ApJ, 756, 111
Maund J. R., Smartt S. J., 2009, Science, 324, 486
Maund J. R., Smartt S. J., Schweizer F., 2005, ApJ, 630, L33
Maund J. R. et al., 2011, ApJ, 739, L37
Maund J. R. et al., 2015, MNRAS, 454, 2580
Mineo S., Gilfanov M., Sunyaev R., 2012, MNRAS, 419, 2095
Mitsuda K. et al., 1984, PASJ, 36, 741
Modjaz M. et al., 2009, ApJ, 702, 226
Monet D. G. et al., 1998, USNO-A2.0., United States Naval Observatory Flagstaff Station and Universities Space Research Association
Nasonova O. G., de Freitas Pacheco J. A., Karachentsev I. D., 2011, A&A, 532, A104
Nazé Y., Rauw G., Hutsemékers D., 2012, A&A, 538, A47
Nelemans G., Voss R., Nielsen M. T. B., Roelofs G., 2010, MNRAS, 405, L71
Nielsen M. T. B., Voss R., Nelemans G., 2012, MNRAS, 426, 2668
Nielsen M. T. B., Voss R., Nelemans G., 2013, MNRAS, 435, 187
Ochsenbein F., Bauer P., Marcout J., 2000, A&AS, 143, 23
Pastorello A. et al., 2008, MNRAS, 389, 955
Paturel G., Petit C., Prugniel P., Theureau G., Rousseau J., Brouty M., Dubois P., Cambrésy L., 2003, A&A, 412, 45
Perna R., Soria R., Pooley D., Stella L., 2008, MNRAS, 384, 1638
Podsiadlowski P., Joss P. C., Hsu J. J. L., 1992, ApJ, 391, 246
Pooley D., Lewin W. H. G., 2003, IAU Circ., 8110, 2
Pounds K. A., King A. R., 2013, MNRAS, 433, 1369
Poutanen J., Fabrika S., Valeev A. F., Sholukhova O., Greiner J., 2013, MNRAS, 432, 506
Poznanski D. et al., 2009, ApJ, 694, 1067
Predehl P., Schmitt J. H. M. M., 1995, A&A, 293, 889
Prieto J. L., Rest A., Suntzeff N. B., 2006, ApJ, 647, 501
Reindl B., Tammann G. A., Sandage A., Saha A., 2005, ApJ, 624, 532
Reynolds T. M., Fraser M., Gilmore G., 2015, MNRAS, 453, 2885
Roming P. W. A. et al., 2009, ApJ, 704, L118
Rupen M. P., Sramek R. A., van Dyk S. D., Weiler K. W., Panagia N., Richmond M. W., Filippenko A. V., Treffers R. R., 1994, IAU Circ., 5963, 1
Russell D. G., 2002, ApJ, 565, 681
Ryder S. D., Sadler E. M., Subrahmanyan R., Weiler K. W., Panagia N., Stockdale C., 2004, MNRAS, 349, 1093
Ryder S. D., Murrowood C. E., Stathakis R. A., 2006, MNRAS, 369, L32
Saha A., Thim F., Tammann G. A., Reindl B., Sandage A., 2006, ApJS, 165, 108
Sana H. et al., 2012, Science, 337, 444
Schlegel E. M., Ryder S., 2002, IAU Circ., 7913, 1
Seward F. D., Charles P. A., Foster D. L., Dickel J. R., Romero P. S., Edwards Z. I., Perry M., Williams R. M., 2012, ApJ, 759, 123
Skrutskie M. F. et al., 2006, AJ, 131, 1163
Smartt S. J., 2009, ARA&A, 47, 63
Smartt S. J., 2015, PASA, 32, 16
Smith N., Li W., Filippenko A. V., Chornock R., 2011, MNRAS, 412, 1522
Soderberg A. M., Kulkarni S. R., Berger E., Chevalier R. A., Frail D. A., Fox D. B., Walker R. C., 2005, ApJ, 621, 908
Soderberg A. M. et al., 2008, Nature, 453, 469
Springob C. M., Masters K. L., Haynes M. P., Giovanelli R., Marinoni C., 2009, ApJS, 182, 474
Svirski G., Nakar E., 2014, ApJ, 788, L14
Takanashi N., Doi M., Yasuda N., 2008, MNRAS, 389, 1577
Terry J. N., Paturel G., Ekholm T., 2002, A&A, 393, 57
Theureau G., Hanski M. O., Coudreau N., Hallet N., Martin J.-M., 2007, A&A, 465, 71
Tsvetkov D. Y., 1985, SvA, 29, 211

Downloaded from http://mnras.oxfordjournals.org/ at University of Turku on February 1, 2016

Tsvetkov D. Y., Pavlyuk N. N., Bartunov O. S., 2004, AstL, 30, 729
Tully R. B., Rizzi L., Shaya E. J., Courtois H. M., Makarov D. I., Jacobs B. A., 2009, AJ, 138, 323
Valenti S. et al., 2011, MNRAS, 416, 3138
Van Dyk S. D., Li W., Filippenko A. V., 2003, PASP, 115, 1
Van Dyk S. D. et al., 2011, ApJ, 741, L28
Vanbeveren D., De Donder E., Van Bever J., Van Rensbergen W., De Loore C., 1998, New Astron., 3, 443
Voss R., Nielsen M. T. B., Nelemans G., Fraser M., Smartt S. J., 2011, MNRAS, 418, L124
Wang X., Wang L., Pain R., Zhou X., Li Z., 2006, ApJ, 645, 488
Weyant A., Wood-Vasey W. M., Allen L., Garnavich P. M., Jha S. W., Joyce R., Matheson T., 2014, ApJ, 784, 105
Wood-Vasey W. M. et al., 2008, ApJ, 689, 377
Yoon S.-C., 2015, PASA, 32, 15
Zezas A., Ward M. J., Murray S. S., 2003, ApJ, 594, L31
Zezas A., Fabbiano G., Baldi A., Schweizer F., King A. R., Ponman T. J., Rots A. H., 2006, ApJS, 166, 211
Zhekov S. A., Gagné M., Skinner S. L., 2011, ApJ, 727, L17

This paper has been typeset from a TEX/LATEX file prepared by the author.

Downloaded from http://mnras.oxfordjournals.org/ at University of Turku on February 1, 2016